LinTT1 peptide-functionalized liposomes for targeted breast cancer therapy

þÿ d Avanzo, Nicola

2021-03-15

þÿ d Avanzo , N , Torrieri , G , Figueiredo , P , Celia , C , Paolino , D , Moslova , K , Teesalu , T , Fresta , M & Santos , H A 2021 , ' LinTT1 peptide-functionalized liposomes for targeted breast cancer therapy ' , International Journal of Pharmaceutics , vol. 597 , 120346 . https://doi.org/10.1016/j.ijpharm.2021.120346

http://hdl.handle.net/10138/328589
https://doi.org/10.1016/j.ijpharm.2021.120346

International Journal of Pharmaceutics 597 (2021) 120346

Contents lists available at ScienceDirect

International Journal of Pharmaceutics

journal homepage: www.elsevier.com/locate/ijpharm

LinTT1 peptide-functionalized liposomes for targeted breast cancer therapy

Nicola d'Avanzo [a,b], Giulia Torrieri [b], Patrícia Figueiredo [b], Christian Celia [c], Donatella Paolino [d], Alexandra Correia [b], Karina Moslova [e], Tambet Teesalu [f], Massimo Fresta [a,*], Hélder A. Santos [b,g,*]

[a] Department of Health Sciences, University of Catanzaro "Magna Græcia", Campus Universitario "S. Venuta", Viale Europa, I-88100 Catanzaro, Italy
[b] Drug Research Program, Division of Pharmaceutical Chemistry and Technology, Faculty of Pharmacy, University of Helsinki, FI-00014 Helsinki, Finland
[c] Department of Pharmacy, University of Chieti-Pescara "G. d'Annunzio", Via dei Vestini 31, I-66100 Chieti, Italy
[d] Department of Experimental and Clinical Medicine, University of Catanzaro "Magna Græcia", Campus Universitario "S. Venuta", Viale Europa, I-88100 Catanzaro, Italy
[e] Department of Chemistry, University of Helsinki, FI-00014 Helsinki, Finland
[f] Laboratory for Cancer Biology, University of Tartu, Tartu 50411, Estonia
[g] Helsinki Institute of Life Science (HiLIFE), University of Helsinki, FI-00014 Helsinki, Finland

ARTICLE INFO

Keywords:
Nanomedicines
Functionalized-liposomes
Breast cancer
Targeted therapy: multidrug approach

ABSTRACT

Breast cancer, with around 2 million new cases in 2019, is the second most common cancer worldwide and the second leading cause of cancer death among females. The aim of this work is to prepare a targeting nanoparticle through the conjugation of LinTT1 peptide, a specific molecule targeting p32 protein overexpressed by breast cancer and cancer associated cells, on liposomes' surface. This approach increases the cytotoxic effects of doxorubicin (DOX) and sorafenib (SRF) co-loaded in therapeutic liposomes on both 2D and 3D breast cancer cellular models. The liposome functionalization leads to a higher interaction with 3D breast cancer spheroids than bare ones. Moreover, interaction studies between LinTT1-functionalized liposomes and M2 primary human macrophages show an internalization of 50% of the total nanovesicles that interact with these cells, while the other 50% results only associated to cell surface. This finding suggests the possibility to use the amount of associated liposomes to enrich the hypoxic tumor area, exploiting the ability of M2 macrophages to accumulate in the central core of tumor mass. These promising results highlight the potential use of DOX and SRF co-loaded LinTT1-functionalized liposomes as nanomedicines for the treatment of breast cancer, especially in triple negative cancer cells.

1. Introduction

Breast cancer is the second most commonly diagnosed cancer worldwide and the second leading cause of cancer death among women (Bray et al., 2018). The statistics indicate that about 16.2% of 850,000 cancer deaths in 2018 in European countries were associated to breast cancer (Dafni et al., 2019), and 279,100 new breast cancer cases are estimated to occur in the United States in 2020 (Siegel et al., 2020). Oncological patients who have been diagnosed with breast cancer can be subjected to different therapies, such as surgery, radiation therapy and chemotherapy, often used in association (Akram et al., 2017). Despite the improved survival rate during the last three decades (DeSantis et al., 2019), mainly due to the early diagnosis (Hawkes, 2019; Wang, 2017) and the development of endocrine and hormone receptor targeted treatments (Masoud and Pagès, 2017; Tremont et al., 2017), conventional chemotherapies still play a crucial role in adjuvant and neo-adjuvant setting (Waks and Winer, 2019), especially in triple negative breast (TNB) cancer that are not responsive to hormonal therapies (Wahba and El-Hadaad, 2015). Unfortunately, conventional chemotherapeutic agents show several restrictions: (i) inadequate

* Corresponding authors at: Drug Research Program, Division of Pharmaceutical Chemistry and Technology, Faculty of Pharmacy, University of Helsinki, FI-00014 Helsinki, Finland (H.A. Santos). Department of Health Sciences, University of Catanzaro "Magna Græcia", Campus Universitario "S. Venuta", Viale Europa, I-88100 Catanzaro, Italy (M. Fresta).

E-mail addresses: nicola.davanzo@unicz.it (N. d'Avanzo), giulia.torrieri@helsinki.fi (G. Torrieri), patricia.figueiredo@helsinki.fi (P. Figueiredo), c.celia@unich.it (C. Celia), paolino@unicz.it (D. Paolino), alexandra.correia@helsinki.fi (A. Correia), karina.moslova@helsinki.fi (K. Moslova), tambet.teesalu@ut.ee (T. Teesalu), fresta@unicz.it (M. Fresta), helder.santos@helsinki.fi (H.A. Santos).

https://doi.org/10.1016/j.ijpharm.2021.120346
Received 30 October 2020; Received in revised form 29 January 2021; Accepted 30 January 2021
Available online 2 February 2021

pharmacokinetic profiles; (ii) physicochemical instability after *in vivo* administration; (iii) the development of resistance mechanisms; and (iv) the poor or lack specificity towards the pathological tissues. These drawbacks lead to several side effects, which strongly compromise the patients' health and decrease their compliance to the therapies, thus making priority the development of a "new generation" of chemotherapeutic agents (Arruebo et al., 2011; Wicki et al., 2015; Du et al., 2019).

In this scenario, the use of nanocarriers as drug delivery systems (DDSs) had a significant impact in cancer therapy, as shown by the presence of nanomedicines that are currently available on the market like Doxil®, Myocet®, Abraxane®, Onivyde® DaunoXome®, Thermo-Dox® and many others in clinical trials for the treatment of breast cancer (Anselmo and Mitragotri, 2019; Di Wu et al., 2017). The use of DDSs overcomes several limitations related to the conventional chemotherapies, by preserving payloads from degradation (Maggisano et al., 2019), providing a sustained and controlled release (Yong et al., 2019; Barone et al., 2019), and increasing the therapeutic efficacy by allowing the selective targeting of nanocarriers to the tumor tissue (Almeida et al., 2014), thus improving the pharmacokinetic profiles (Unnam et al., 2019; Celia et al., 2021) and decreasing the administration frequency of drug dosage (Bulbake et al., 2017).

In particular, liposomes have been widely studied as drug delivery systems for anticancer use due to their biocompatibility (Wolfram et al., 2014a,b), the high formulation versatility that provides a nanoplatform to the delivery of hydrophilic and lipophilic payloads (as single agents or combination) (Cosco et al., 2012) and the opportunity to modify their physicochemical characteristics, such as size, surface properties and composition (Olusanya et al., 2018). These last features can be opportunely optimized in order to take advantage from pathophysiological changes that occur into the tumor microenvironment (TME), increasing the nanoparticle specificity (Olusanya et al., 2018).

Liposomes can be properly modified, by conjugating directly to phospholipids and/or polymers (Riaz et al., 2018) specific ligands capable to target selectively receptors overexpressed in TME components, thus improving their accumulation inside the tumor tissue and increasing their therapeutic effects (Paolino et al., 2014; Luo et al., 2020). To date, several molecules, i.e. antibodies, peptides and proteins, are used to modify the surface of DDSs and provide targeted breast cancer therapies (Khan et al., 2015). In particular, tumor homing peptides are one of the most promising strategies in this field (Singh et al., 2019; Qu et al., 2017). These molecules consist of <30 amino acids and are accumulated in the tumor tissues, providing a potential use as specific targeting and diagnostic agents in cancer therapy (Laakkonen and Vuorinen, 2010). These peptides have several advantages compared to other targeting molecules, such as higher tumor penetrating properties than conventional antibodies, cheap synthetic process, higher selectivity than small targeting molecules, i.e. aptamers, and non-immunogenic properties (Vlieghe et al., 2010). In these attempts, the *trans*-membrane gC1q receptor (gC1qR), also known as p32 protein, is one of the most promising molecules to target aggressive adenocarcinoma, such as breast cancer (Saha and Datta, 2018; Peerschke and Ghebrehiwet, 2014; Rubinstein et al., 2004). The protein p32 is over-expressed on the cellular surface of cancer (Rubinstein et al., 2004; Fogal et al., 2008) and tumor associated cells, like active angiogenic endothelial cells, cancer associated fibroblast, and tumor associated macrophages (TAMs) (Agemy et al., 2013; Sharma et al., 2017). The protein p32 is further overexpressed in malignant cancers (Peerschke et al., 2019) and play a crucial role in tumor progression (Saha and Datta, 2018; Chen et al., 2009). These results demonstrated that p32 protein is a new target for breast cancer, and particularly TNB cancers, where the common receptors that are currently used for targeted therapy are lacking (Khosravi-Shahi et al., 2019).

Linear TT1 (LinTT1) peptide (AKRGARSTA), a specific molecule targeting p32 protein (Simón-Gracia et al., 2018b; Simón-Gracia et al., 2018a), was used in this study to modify the surface of liposomes. As a result of its lower affinity for p32 protein in comparison with parental disulfide-bridged cyclic TT1 peptide, it showed a limited interaction with the receptor located on "binding-site barrier" in the TME, resulting in an increased extravasation and a significant accumulation in inner tumor tissues (Sharma et al., 2017). Furthermore, as previously demonstrated *in vivo*, urokinase-type plasminogen activator (uPA), a serine protease aberrantly expressed in malignant tumor, makes the cleavage of LinTT1 peptide, leading to the exposition of C-end moiety (AKRGAR) (Simón-Gracia et al., 2018b; Braun et al., 2016). This C-end Rule (CendR) motif binds the transmembrane receptor Neuropilin-1 (NRP-1) wich results over-expressed in tumor tissue, leading to an improved penetration of the peptide and conjugated-cargo into the tumor (Simón-Gracia et al., 2018b).

The aim of this work was the design and synthesis of therapeutic targeting liposomes through the conjugation of LinTT1 peptide onto the surface of preformed liposomes. The resulting functionalized liposomes were physicochemically characterized and the conjugation of peptide to liposomal surface was measured by elemental and fluorescent analysis, while blood safety was evaluated using human red blood cells (RBCs). Sorafenib (SRF) and doxorubicin hydrochloride (DOX) were co-loaded inside the LinTT1-functionalized liposomes (LinTT1-Lipo) to provide a synergistic effect of the two drugs, and improve the cytotoxic activity of liposomal doxorubicin (Doxil®/Caelyx® or Myocet®) that is currently on market and used in clinic. Despite SRF is currently approved for hepatocellular (Keating, 2017), iodine resistant thyroid (Pitoia and Jerkovich, 2016) and renal cell carcinoma (Wilhelm et al., 2006), several studies demonstrated its efficacy in breast cancer therapies when it was co-administered with other drugs which are commonly used in breast anticancer therapy (Lei et al., 2019; Chen et al., 2019a). The anticancer activity of therapeutic LinTT1-Lipo was evaluated on both 2D (MCF-7 and MDA-MB-231 cells) and 3-D (MDA-MB-231) cancer cell models. The interaction between LinTT1-Lipo and 3D spheroids was evaluated *in vitro* by flow cytometry and confocal laser scanning microscopy analyses. Finally, the interaction between LinTT1-Lipo and primary human M2 macrophages was also studied. TAMs are commonly present in TME and play a crucial role in cancer progression (Chen et al., 2019b). In response to the physical stimuli in TME, such as hypoxia in the tumor core area and the high levels of chemokine, i.e. IL-4, TAMs population is off-balanced toward M2-phenothype, thus showing oncogenic properties (Chen et al., 2019b; Park et al., 2019). For these reasons, the targeting of TAMs is one of the most promising approaches to prepare innovative anticancer nanomedicines (Cassetta and Pollard, 2018). In this investigation, we focused our efforts on the opportunity to use these cells to increase the liposomes accumulation in tumor core through a "cellular hitchhiking" approach (Torrieri et al., 2020). We hypothesize that this approach and the intrinsic ability of these cells to accumulate in the central area of the solid tumor, could increase the drug concentration in the hypoxic tumor tissue where anticancer therapy with drug delivery systems that are currently used have failed so far.

2. Materials and methods

2.1. Materials

Cholesterol (CHOL), trypan blue solution and polysorbate 80 (Tw80) were obtained from Sigma-Aldrich. 1,2- dipalmitoyl-*sn-glycero*-3-phospocholine (DPPC), N-(carbonyl-methoxypolyethylene glycol-2000)-1,2-distearoylsn-*glycero*-3 phosphoethanolamine (DSPE-mPEG2k), 1,2-distearoyl-*sn-glycero*-3-phosphoethanolamine-N-[maleimide (polyethylene glycol)-2000] (DSPE-PEG2000mal) and Ganglioside were purchased from Avanti Polar (Suffolk, UK). Doxorubicin hydrochloride (DOX) was provided from Tokyo Chemical Industry Co. Ltd, Japan. Hank's balance salt solution (HBSS), trypsin, Dulbecco's modified Eagle's medium (DMEM), Rosewell Park Memorial Institute (RPMI) culture-medium, penicillin–streptomycin (PEST), L-glutamine, fetal bovine serum (FBS), non-essential amino acids (NEAA) and phosphate buffered saline (PBS) solution were provided from HyClone (USA). N-(fluorescein-5-

tiocarbamoyl)-1,2-dihexadecanoyl-*sn-glycero*-3-phosphoethanolamine triethylammonium salt (fluorescein-DHPE) and DAPI-405 were purchased from Thermo Fisher Scientific Co. (St. Louis, USA). Sorafenib (SRF) was obtained from LC laboratories® (USA). Paraformaldehyde (PFA) was purchased from Sigma-Aldrich,USA. Ficoll-Paque was obtained from GE Healthcare Bio-sciences (Piscataway, NJ). All the other reagents used in the experiments were of analytical grade.

Human breast cancer cell lines (MDA-MB-231 and MCF-7) and human Foreskin fibroblast cell lines were obtained from American Type Culture Collection (ATCC), USA. Red blood cells and M2 macrophages were collected starting from Heparin-stabilized fresh human blood provided by the Finnish Red Cross Blood Service by anonymous donors.

2.2. Synthesis of LinTT1-liposomes

Liposomes were synthesized using the thin layer evaporation (TLE) method (Paolino et al., 2014). Briefly, lipids were dissolved in round-bottomed vials using an organic solvent mixture (chloroform/methanol 3:1 v/v). The final lipid molar ratio was 6:3:0.6:0.4 for DPPC:CHOL:GANGLIOSIDE:DSPEmPEG2000-maleimmide, respectively. The organic solvents were removed using a rotavapor Büchi R-210 at 40 °C (Flawil, Switzerland) and the residual solvent was dried overnight by a Büchi T51 glass drying oven (Flawil, Switzerland) connected to a vacuum pump. The resulting lipid film was hydrated with a PBS solution (10 mM, pH 7.4) to obtain a final lipid concentration of 20 mg mL^{-1}. Three alternate cycles (3 min each) of warming at 60 °C, in a thermostatic water bath, and vigorous mixing, by vortex at 750 rpm, were used during the hydration process. The resulting multilamellar liposomes were kept at 60 °C for 1 h to anneal the bilayer structure and then extruded by a Lipex extruder at 60 °C (Vancouver, Canada) through polycarbonate membrane filters with pore sizes from 800 to 100 nm (Nucleopore® Polycarbonate). After extrusion, the liposomal suspension was incubated with a PBS solution (10 mM, pH 7.4) containing LinTT1 peptide (lipid:peptide ratio at 60:1 w/w) for 3 h at room temperature under continuous magnetic stirring (≈200 rpm). The obtained LinTT1-functionalized liposomes (LinTT1-Lipo) was purified by Amicon® Ultra centrifugal filters (cut-off 100 kDa, 13000 rpm for 5 min) and washed twice with fresh PBS solution (10 mM, pH 7.4).

To obtain therapeutic LinTT1-functionalized liposomes, SRF, if necessary, was added to lipid mixture with a final concentration of 0.5 mg mL^{-1} of drug per final volume of liposomes, while DOX was entrapped using a pH gradient and remote loading procedure (Barenholz, 2012). Briefly, for DOX loading, lipid film hydration was obtained using an ammonium sulphate solution (250 mM, pH 5.5), followed by warming and extrusion, as described above. After extrusion, liposomes were centrifuged at 90,000g for 1 h, at 4 °C by using a Beckman Optima™ Ultracentrifuge (Fullerton, Canada). The resulting pellet was re-suspended with a DOX solution to have a final drug concentration of 1 mg mL^{-1} (PBS 10 mM, pH 7.4). The samples were then heated for 1 h up to the transition temperature or Tm (60 °C), and under continuous stirring to facilitate the DOX crystallization in the aqueous core of liposomes. The unentrapped DOX was removed by a dialysis tube (cut-off 10,000 Da, Spectrum Labs, Breda, Netherlands) under continuous slowly stirring at room temperature for 2 h. A fresh PBS solution (10 mM; pH 7.4) was used as receptor medium. Then the peptide was conjugated to therapeutic liposomes, as described above.

Unconjugated liposomes (bare-Lipo) were synthetized using the same procedures as described above by replacing DSPEmPEG 2000-maleimide with DSPEmPEG2000 at the same molar ratio. When required, fluorescent liposomes were obtained by adding DHPE-fluorescein (0.1% w/w) to the lipid mixture of bare-Lipo during the preparation procedure, while LinTT1-functionalized liposomes were per se fluorescent due to FAM group included in the backbone structure of the peptide.

2.3. Physicochemical characterization

The average hydrodynamic diameter, polydispersity index (PDI) and zeta-potential were measured with a Zetasizer Nano ZS (Malvern Instruments Ltd, Malvern, UK), set with a 4.5 mW laser diode, operating at 670 nm, and a detection angle of 173°. Samples were properly diluted 50-folds with PBS or MilliQ-water for size and zeta-potential analyses, to avoid multi-scattering phenomena. Results were expressed as the average of three different experiments ± S.D. Moreover, the concentration of nanovesicles (liposomes/mL) was quantified by using Zetasizer Ultra (Malvern Panalytical Instruments Ltd, Malvern, UK) and this parameter was used to calculate the density of LinTT1 conjugated to liposomal surface.

FTIR analysis was obtained on freeze-dried liposomes using a FTIR instrument (Vertex 70, Bruker, USA). The resulting ATR-FTIR spectra were recorded between 3600 and 700 cm^{-1} with a resolution of 4 cm^{-1} using an OPUS 5.5 software, at room temperature.

The elemental composition of bare-Lipo and LinTT1-Lipo, for the relative percentages of carbon (C), hydrogen (H), nitrogen (N) and sulfur (S), was measured on freeze-dried samples by using a Vario MICRO cube CHNS analyzer (Elementar Analysensysteme GmbH, Langenselbold, Germany). Different nitrogen percentage amounts between the two samples were used to confirm the conjugation of LinTT1 on the surface of liposomes via PEG. The instrument was daily calibrated through sulphanilamide, that is the recommended calibration standard to calculate the systematic error for each analysis (Vergallo et al., 2020).

The successful conjugation of LinTT1 peptide was also confirmed by a Varioskan™ LUX multimode microplate reader (Thermo Fisher Scientific Inc., USA). Briefly, after purification the fluorescence of LinTT1 peptide was measured after its conjugation to liposomal surface and the analysis was carried out by measuring the fluorescence of 5-FAM group that is included in the backbone structure of peptide. Data was compared with fluorescent signals of bare-Lipo. A wavelength of 495 and 515 nm were used as excitation and emission wavelength, respectively, during the analysis.

Finally, the peptide's conjugation efficiency on liposomes surface, was also evaluated in a fluorescent mode, using a suitable calibration curve (Figure S1).

TEM analysis was carried out, as described elsewhere (Barone et al., 2020). Briefly, liposomes were appropriately diluted (1:200, v/v) in isotonic and inert buffer, and then deposited on 200-mesh formvar-coated copper grid (TABB Laboratories Equipment, UK). The resulting samples were stained by uranyl acetate solution (2%, w/v) and then dried at 23 °C. The images were acquired using a JEM 2010 microscope (Jeol, MA, USA) (Figure S2 and S3).

2.4. NMR analysis

The conjugation of LinTT1 to DSPE-PEG2000mal by sulfhydryl-maleimide reaction was tested by ^{1}H NMR, as reported elsewhere with some modifications (Wang et al, 2019). Briefly, LinTT1 was dissolved in PBS (pH = 7.4, 10 mM), while DSPE-PEG2000mal was dissolved in N,N dimethylformamide (DMF). The resulting lipid solution was then added to the LinTT1 solution under continuous magnetic stirring at room temperature. The final molar ratio between peptide and DSPE-PEG2000mal was 1.5:1. After 3 h of incubation, the excess of DMF and unconjugated peptide was removed by dialysis using a dialysis tube of 3.5 kDa (Spectra/Por 1 Standard RC Dry Dialysis Tubing, Spectrum Labs, USA.) versus deionized water. The dialysis was carried out at room temperature for 6 h. The resulting product was freeze-dried (Christ Alpha 1–4 LCG, Osterode am Harz Germany), and then analyzed by Varian Mercury 300 MHz instrument (Varian Inc., Palo Alto, CA, USA). The analysis was carried out according to manufacture instructions and software set-up of both instruments, and ^{1}H NMR of LinTT1, DSPE-PEGmal, and DSPE-PEGmal-LinTT1 was analyzed (Figure S4).

2.5. Hemocompatibility test

Red blood cells (RBCs) were isolated starting from whole human blood and used to evaluate the hemocompatibility of LinTT1-functionalized liposomes, as reported elsewhere (Shahbazi et al., 2013; Yu et al., 2011; Bhatt et al., 2018). Briefly, RBCs were washed for five times with sterile PBS (10 mM, pH 7.4). About 2 mL of cell suspension was then diluted up to 40 mL with PBS (≈5% hematocrit). This diluted RBC suspension (0.1 mL) was added to LinTT1-Lipo (0.4 mL) that has been previously diluted with PBS in order to have a final lipid concentration of 25, 50, 100, and 200 μg mL^{-1}. The resulting suspension was gently mixed and then incubated under continuous shaking at 37 °C, for 48 h. At fixed time points (1, 4, 8, 12, 24, and 48 h), samples were vortexed again and centrifuged for 5 min at 13,000 rpm. For each time point, 100 μL of the supernatant were transferred to a 96-well plate and the absorbance of hemoglobin was measured at 577 nm, using a reference wavelength of 655 nm. The analysis was carried out by a Varioskan™ LUX multimode microplate reader (Thermo Fisher Scientific Inc., USA). MilliQ-water and PBS solution (0.4 mL) were used as positive and negative controls, respectively, during the analysis.

2.6. Drugs loading capability and in vitro release kinetic of liposomes

Liposomes were lyophilized and then disrupted with cooled absolute methanol and the amount of DOX and/or SRF entrapped inside liposomes were evaluated by Varioskan™ LUX multimode microplate reader (Thermo Fisher Scientific Inc., USA) and HPLC, respectively. Empty liposomes with the same lipid composition were used as blank during the analysis. For both drugs, the entrapment efficiency (E.E.%) and drug loading (D.L.%) were evaluated, according to Equations (1) and (2):

$$\boldsymbol{E.E.\%} = \frac{\boldsymbol{D_{en}}}{\boldsymbol{D_{tot}}} \times 100 \quad (1)$$

$$\boldsymbol{D.L.\%} = \frac{\mathbf{D_{en}}}{\mathbf{L_w}} \times 100 \quad (2)$$

where, D_{en} is the amount of encapsulated drug, D_{tot} is the total amount of drug added during preparation procedure and L_w is the amount of lipids used to make liposomes. The HPLC analysis for SRF quantification was performed, as reported elsewhere (Almeida et al., 2017). The analysis was carried out using a C_{18} column (4.6 × 100 mm, 3 μm, Gemini-Nx plus C18; Phenomenex, CA, USA) at room temperature. The mobile phase consisted of 0.2% (v/v) of trifluoroacetic (TFA) acid buffer (pH 2) and acetonitrile (42:58 v/v ratio), and the flow rate was set at 1.0 mL min^{-1}. For each sample, 20 μlL was injected and SRF was detected at the maximum wavelength of 254 nm. For DOX quantification, 100 μL of disrupted liposomes were placed in a 96-well plate and drug was detected by a Varioskan™ LUX multimode microplate reader (Thermo Fisher Scientific Inc., USA) in a fluorescent mode (λ_{ex} 470 nm; λ_{em} 585 nm). An appropriate external calibration curve for each drug was used to calculate the amount of DOX and SRF entrapped inside the liposomes (Figure S5). SRF amount to be included in the lipid bilayer of liposomes was studied and the one that provided the maximum drug loading efficiency percentage (Figure S6), was selected for further studies.

In vitro drug release of DOX and SRF co-loaded into LinTT1-functionalized liposomes (LinTT1-Lipo/D + S) was evaluated by the dialysis bag method, using a cellulose acetate dialysis tube (Spectra/Por 1 Standard RC Dry Dialysis Tubing, 12–14 kDa, Spectrum Labs, USA.). Two different solutions were used as receptor medium for DOX and SRF: PBS solution supplemented with 1% (v/v) of Tw80 and PBS solution supplemented with 10% of FBS. The receptor medium was adjusted to have a final pH of 7.4, 6.5 and 5.5. Liposomes (1 mL) were placed in the dialysis bag and transferred into a beaker containing 100 mL of the receptor medium. The release medium was constantly warmed (37 ± 0.5 °C) and gently stirred up to 72 h of incubation (GR 150 thermostat, Grant Instruments Ltd., Cambridge, UK). At fixed time points, 1 mL of receptor medium was withdrawn and replaced with the same volume of fresh fluid. Samples were then analyzed by HPLC and by Varioskan™ LUX multimode microplate reader (Thermo Fisher Scientific Inc., USA) for SRF and DOX, respectively. To remove the autofluorescence of serum proteins, and thus, prevent potential interferences during the analysis, the collected samples were pre-treated, as reported elsewhere (Charrois and Allen, 2004; Di Francesco et al., 2021). Briefly, samples were mixed with slight acid methanol (sample/methanol 1:3, v/v, ratio) and then stirred for 1 min. The resulting mixture was then centrifuged (11,500*g* for 10 min) and the supernatant was used for the analysis. A sample containing only the receptor medium was used as blank for different media and pH values to normalize the resulting data. Equation (3) was used to calculate the percentage of released drugs:

$$\textbf{Drug released}\% = \left(\frac{\mathbf{drug_{rel}}}{\mathbf{drug_{load}}} \times \mathbf{d.f.}\right) \times 100 \quad (3)$$

where, $drug_{rel}$ is the amount of drug released at selected time point, $drug_{load}$ is the amount of drug entrapped inside liposomes and d.f. is the dilution factor that was used during the analysis. To optimize results, the drug release was calculated using the appropriate external calibration curves consisting of the same buffer used during release studies (composition and pH values) of DOX and SRF (Figure S7 and S8). Results are the average of three independent experiments ± S.D.

2.7. Stability studies in human plasma.

The human plasma stability of DOX/SRF-co-loaded LinTT1-functionalized liposomes was tested with some modifications, as previously reported elsewhere (Almeida et al., 2014). The human plasma was purified starting from the whole human blood obtained from anonymous donors through the Finnish Red Cross Blood Service. The human plasma was isolated and collected as reported in the *Section 2.11* and stored at − 20 °C until the day of experiment. Briefly, 400 μL of DOX/SRF-co-loaded LinTT1-functionalized liposomes were incubated with 2 mL of medium (saline solution NaCl 0.9%/human plasma, 50:50 (v/v)) at 37 °C. The resulting mixture was maintained under continuous stirring (300 rpm) up to 72 h. At fixed time points (30 min, 1 h, 2 h, 4 h, 6 h, 8 h, 24 h, 48 h, 72 h) 100 μL of samples was withdrawn and its relative average size (liposomes) was measured by DLS. The resulting data was compared to that obtained for HSPC:Chol:DSPE-PEG2000 (6.5:3:0.5 lipid molar ratio) loading DOX (2 mg/mL) (Caelyx-like Lipo) which is similar to Doxil/Caelyx commercial liposomes. The incubation of liposomes with saline solution (0.9% NaCl) was used as negative control (data not shown).

The stability of DOX/SRF-co-loaded LinTT1-functionalized liposomes and Caelyx-like Lipo (control) was analyzed using Turbiscan Lab® Expert (L'Union, France), which can predict the potential destabilization phenomena (sedimentation, coagulation or flocculation) of intact liposomes and colloidal nanocarriers in general, as reported elsewhere (Caddeo et al., 2018; Tai et al., 2018). Turbiscan Lab® Expert analysis was used to test how the human plasma can affect the stability of DOX/SRF-co-loaded LinTT1-functionalized liposomes and Caelyx-like Lipo (control). Briefly, 600 μL of liposomes were diluted up to 6 mL with medium (saline solution NaCl 0.9%/human plasma, 50:50 (v/v)) or with saline solution (NaCl 0.9%), as a negative control. The resulting mixtures were then placed into a glass tube and analyzed for 1 h. The analysis was carried out at 37 °C, which is equivalent to body temperature, using a pulsed near infrared LED (wavelength set at 880 nm). Significant variation of Back Scattering (ΔBS) and Transmission (ΔT) signals *vs* sample height (Figura S9 and S10) were used to test the potential destabilization phenomena of liposomes (Celia et al., 2009). Moreover, the destabilization kinetic profile *vs* incubation time was further evaluated (Figure S11).

2.8. 3D tumor spheroids preparation

3D spheroids of MDA-MB-231 cells were obtained using the bioprinting method, as previously described (Figueiredo et al., 2019), with some modifications. Briefly, MDA-MB-231 and human Foreskin fibroblast cell lines were seeded in 6-well plates at density of 4×10^5 cells per well and left to attach overnight. Afterwards, each well was treated with 50 μL of NanoShuttle-PL (Nano3D Biosciences Inc., Germany) and incubated for 10 h. After incubation time, cells were washed with sterile PBS, detached by trypsin and mixed again to obtain a final number ratio of 8:2 for cancer cells and fibroblast, respectively. The cell mixture was then seeded in ultralow attachment 96-well plates at a density of 8×10^3 cells per well and the resulting plate was placed on the top of 96-well spheroid magnetic drive for 15 h (Nano3D Biosciences Inc., Germany). Cells aggregated under a magnetic field and the resulting spheroids were cultured for 2 days before the treatment.

2.9. In vitro cytotoxic studies

The cytotoxic effects of DOX, with or without SRF, as free drugs and entrapped in bare or in LinTT1-functionalized liposomes, were evaluated using 3D and 2D cellular models.

For 2D cell models, MCF-7 and MDA-MB-231 breast cancer cell lines were used. Cells were placed in 96-well plates (8×10^3 cells per well) and allowed to attach overnight at 37 °C. The culture medium was then removed, replaced with medium containing therapeutic bare and LinTT1-functionalized liposomes, with a final DOX concentration from 0.01 to 10 μM and incubated for 24, 48 and 72 h. Based on the relative drug loading percentage (%), the SRF concentration tested during the experiments, at different incubation times, was one third of the DOX. CellTiter-GloR® luminescence cell viability assay kit (Promega Corporation, USA) was used to calculate the cell viability percentage (%), according to the Equation (4). Luminescence was evaluated by Varioskan™ LUX multimode microplate reader (Thermo Fisher Scientific Inc., USA).

$$\textbf{Cell viability}(\%) = \frac{\textbf{Lum}_\textbf{T}}{\textbf{Lum}_\textbf{C}} \times 100 \quad (4)$$

where Lum_T is the luminescence associated to treated cells and Lum_c is the luminescence associated to untreated cells (negative control).

For 3D cell model, spheroids of MDA-MB-231 cells, obtained as described above, were gently transferred to 96-well plates (PerkinElmer Inc., USA) and the cell viability was evaluated by using a RealTime-Glo™ MT Cell Viability Assay. Briefly, DOX and SRF as free drugs or co-loaded into bare- and LinTT1-Lipo, were diluted in 50 μL of culture medium and mixed with 50 μL of cell culture medium containing NanoLuc luciferase and MT Cell Viability Substrate. Drugs, both in free form or co-loaded into liposomes, were tested at the same range of concentration that was used for 2D cell culture models. The analysis was carried out at different time points (6, 24, 48 and 72 h). The luminescence was measured using a Varioskan™ LUX multimode microplate reader (Thermo Fisher Scientific Inc., USA), at different incubation times. The cell viability percentage (%) was calculated according to Equation (4). All the experiments for 2D and 3D cellular models were performed in triplicate, and results are expressed as the average ± S.D.

2.10. 3D spheroids and liposomes interaction studies

Interactions between 3D spheroids of MDA-MB-231 cells and liposomes were quantitatively and qualitatively evaluated by flow cytometry and confocal laser scanning microscopy, respectively. 3D spheroids of MDA-MB-231 cells were washed with fresh PBS and then incubated with culture medium containing fluorescent bare-Lipo or LinTT1-Lipo with a final lipid concentration of 500 μg mL^{-1} for 3 and 6 h.

For flow cytometry analysis, 3D spheroids of MDA-MB-231 cells were firstly incubated with fluorescent bare- and LinTT1-Lipo, and then, after suitable incubation times, were harvested for 5 min with trypsin-PBS-EDTA, collected by centrifugation at 1,500 RCF for 5 min and washed twice with PBS solution. The resulting cell suspension was incubated with trypan blue solution (0.005% v/v) for 4 min, then washed twice with PBS-EDTA and re-suspended with fresh PBS-EDTA. The analysis was carried out using LSR II flow cytometer (BD Biosciences, USA), with FACS Diva software. At least 5,000 events were collected for each sample, and data was analyzed by FlowJo VX software (Tree Star, Ashland, OR, USA). All experiments were performed in triplicate.

For confocal laser scanning microscopy analysis, 3D spheroids were treated with fluorescent bare- and LinTT1-Lipo, and then, after incubation times, the cells were washed twice with PBS solution. 3D spheroids of MDA-MB-231 cells were fixed for 24 h at 37 °C using PFA (4% v/v). 3D spheroids of MDA-MB-231 cells were then washed with PBS solution and the nuclei were stained by adding of DAPI-405 (100 μL; 2.8 μg mL^{-1}) and then incubated again for 24 h at 37 °C. Afterward, 3D spheroids of MDA-MB-231 cells were further washed twice with PBS and the localization of bare and LinTT1-functionalized liposomes was observed with a Leica SP5 inverted confocal microscope (Leica Microsystems, Germany), equipped with a 20 × objective.

2.11. Isolation of $CD14^+$ peripheral blood mononuclear cells (PBMC) from whole human blood and polarization of M2 macrophage

Monocytes were isolated from the whole human blood and polarized in M2 macrophage, as reported elsewhere (Torrieri et al., 2020). Briefly, the whole human blood, collected from anonymous donors of the Finnish Red Cross Blood Service and used within 2 h, was diluted with an equal volume of PBS (10 mM, pH 7.4) at room temperature. About 20 mL of diluted blood was layered over 15 mL of Ficoll®-Paque solution in a falcon tube to separate blood constituents through density gradient centrifugation at 400g for 40 min at room temperature. Afterward, RBCs were stored at 4 °C and used for hemocompatibility test, while the PBMCs (the middle layer on the interface between plasma and Ficoll solution) were transferred in new falcon tubes and washed with fresh PBS buffer. The supernatant was discarded, and the pelleted cells were re-suspended in 5 mL of magnetic-activated cell sorting (MACS) buffer. After counting, $CD14^+$ monocytes were isolated from PBMCs by magnetic labeling using MAb CD14 conjugated microbeads (Miltenyi, Biotech, GmBH, USA), followed by physical separation through magnetic column, according to manufacturers' instructions. $CD14^+$ monocytes obtained were seeded in a petri capsule at a density of 2×10^6 cells per 10 mL of Roswell Park Memorial Institute (RPMI) 1640 medium supplemented with 10% of FBS. To promote the differentiation in M2 macrophage, RPMI medium was further supplemented with cytokines macrophage colony-stimulating factor (M−CSF) at the final concentration of 20 ng mL^{-1}. After three days the medium was removed and replaced with a fresh one with the same composition. At day 6 cells were washed twice, detached with PBS/EDTA solution (EDTA concentration 5 mM), centrifuged at 500g for 5 min, re-suspended with RPMI medium, and seeded in 12-well plates at the density of 2.5×10^5 cells per well for flow cytometry analysis. For each well the medium was supplemented with 20 ng mL^{-1} of interleukin 4 (IL-4). Three wells for each plate were supplemented only with 20 ng mL^{-1} of M−CSF and were used as negative control during the analysis (MØ macrophages). On day 8, the markers expression was evaluated in order to confirm the macrophage differentiation. The successful polarization of M2 macrophages was evaluated by flow cytometer analysis using two different fluorescent human antibodies: allophycocyanin (APC)-CD86 and fluorescein isothiocyanate (FITC)-CD206. The two antibodies were incubated with cells for 15 min at 4 °C, and then washed twice to remove the unconjugated antibodies. The expression of two markers was evaluated through LSR II flow cytometer (BD Biosciences, USA). Analyses were performed in triplicate and MØ macrophages were used as control. Finally, at day 9, the interaction between human M2 macrophages and

bare and LinTT1-functionalized liposomes was evaluated.

2.12. Human M2 macrophage-liposomes interaction studies

Flow cytometry analysis was used to study the interaction between primary human macrophages, and bare and LinTT1-functionalized liposomes. Briefly, after polarization, M2 macrophages were seeded in 12-well plates at a density of 2×10^5 cells per well overnight. After removing the cell culture medium, the wells were washed once with PBS solution (pH 7.4). Then, 1.5 mL of bare and LinTT1-functionalized liposomes, with a final lipid concentration of 250 μg per well, were incubated with the cells for 1 and 3 h at 37 °C. Cells were washed twice with PBS solution and then harvested with PBS-EDTA solution. The resulting cell suspensions were centrifuged and washed with PBS buffer three times, and then pelleted cells were re-suspended in an appropriate volume of PBS-EDTA solution for flow cytometer analysis. The interaction extent between liposomes (both bare- and LinTT1-Lipo) and M2 macrophages were evaluated without and with trypan blue solution (0.005% v/v) that was used as cell membrane quencher agent during the experiments. When required, trypan blue solution was incubated with cell suspension for 4 min and then washed twice with PBS-EDTA solution. The analysis was performed with an LSR II flow cytometer (BD Biosciences, USA). Data were analyzed using Flowjo VX software (Tree Star, Ashland, OR, USA).

2.13. Statistical analysis

One-way analysis of variance (ANOVA), followed by Tukey's multiple comparison test was used to analyze the significant difference among results. The analysis was carried out using SigmaPlot v.12 and Excel (Office 2010). Probabilities were set at three different significance levels: *p < 0.05; **p < 0.01 and ***p < 0.001.

3. Results and discussion

3.1. Physicochemical characterization

Physicochemical properties, such as size, zeta-potential and size distribution play a crucial role to design DDSs, particularly on colloidal nanoparticles suitable for a potential systemic administration (Zhao et al., 2019). In this investigation, we analyzed the physicochemical properties of LinTT1-Lipo using dynamic light scattering technique. The average diameter of bare-Lipo and LinTT1-Lipo were 121 ± 3 nm and 146 ± 4 nm, respectively. The increased hydrodynamic radius of LinTT1-Lipo depends on the presence of an additional hydrophilic molecule (LinTT1 peptide) conjugated onto the surface of liposomes (Fig. 1A) (Paolino et al., 2014). LinTT1 peptide also increased the zeta-potential value of liposomes changing from −49.4 ± 3.1 (bare-Lipo) to −32.6 ± 2.3 mV (LinTT1-Lipo) (Fig. 1A). Differences on zeta-potential values between bare and functionalized liposomes may depend on the cationic aminoacids, i.e. arginine and lysine, present on the peptide's structure. The presence of a guanidinium group and an additional amino group in arginine and lysine backbone, respectively, may provide a slight positive zeta-potential value to the free peptide, increasing the overall zeta-potential value of nanosystem after peptide's conjugation to the liposomal surface. Conversely, there was no significant modification of the polydispersity index (PDI) between bare-Lipo and LinTT1-Lipo, having a narrow size distribution with a PDI<0.2 for both formulations (Wolfram et al., 2014a) (Fig. 1A). This is in agreement with data previously reported elsewhere, that demonstrated for other types of nonosystems, a similar PDI before and after functionalization with LinTT1 peptide (Simón-Gracia et al., 2018b). Moreover, the ganglioside

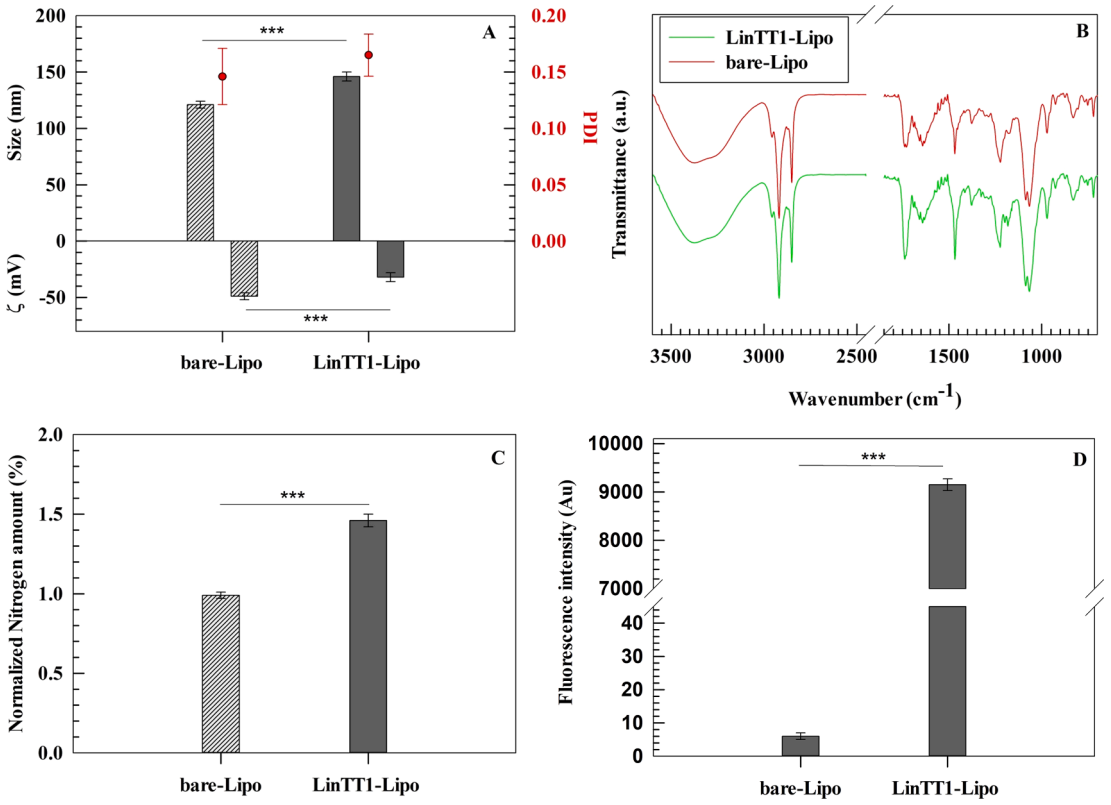

Fig. 1. Physicochemical properties of liposomes evaluated before and after conjugation of LinTT1. (A) Average hydrodynamic diameter, PDI, and zeta-potential value (ζ). (B) ATR-FTIR spectra of bare and LinTT1-functionalized liposomes. (C) Nitrogen amount quantification by elemental analysis of liposomes. (D) Fluorescent intensity of bare and LinTT1-functionalized liposomes. Results are the average of three independent experiments ± standard deviation (S.D.). Statistical significance was obtained by a *p < 0.05, **p < 0.01, and ***p < 0.001.

was used to synthesize liposomal formulations in order to reduce the potential immunogenicity of PEG (d'Avanzo et al., 2020; Mima et al., 2017). Indeed, despite this study is focused on *in vitro* analysis, nanovesicles were optimized for a potential *in vivo* application. Based on this evidence, ganglioside was used to make liposomes and data demonstrated that the presence of this molecule in liposomal structure did not modify the stability of nanovesicles *in vitro*.

Attenuated total reflectance – Fourier transform infrared (ATR-FTIR) analysis demonstrated a more intense carboxylic acid-indicative band at 1745 cm^{-1} (carboxylic acid C = O stretching) in LinTT1-Lipo than bare-Lipo, thus suggesting the presence of a greater number of carboxylic groups on liposomes' surface, after peptide's conjugation. Moreover, the absence of the specific thiol-indicative band at 2550–2600 cm^{-1} (S-H stretching) in both formulations evidenced the lack of free thiolic groups in LinTT1-Lipo, hence confirming the reaction between thiolic group of cysteine in the peptide structure and the maleimide group of polyglycol ethylene (PEG) residual. Nevertheless, in agreement with data reported elsewhere (Torrieri et al., 2020) for LinTT1-functionalized dextran nanoparticles, the conjugation of LinTT1 peptide to the liposomal surface did not significantly modify the FTIR spectrum (Fig. 1B), making it necessary the use of further techniques to confirm the peptide conjugation.

For this, the conjugation of LinTT1 on the surface of liposomes was further studied using elemental composition analysis, which showed a significant increase of the nitrogen amount in LinTT1-Lipo compared to bare-Lipo (Fig. 1C). This finding demonstrated that LinTT1 was successfully conjugated onto the liposomes' surface due to the large number of nitrogen atoms found in the peptide structure. Furthermore, in response to the presence of carboxy-fluorescein group (FAM) in the peptide structure, LinTT1-Lipo showed fluorescent properties (Fig. 1D). The resulting LinTT1-functionalized liposomes had a final peptide amount of 2.59×10^4 peptides/liposomes which corresponds to a density of ~ 0.66 peptide molecules/nm^2. The resulting peptide density, which has been reported as number of peptide molecules/nm^2 of liposomal surface, was very similar to data published by Simón-Gracia in a previous work (0.7 peptide molecules/nm^2 for LinTT1-funtionalized polymersomes), thus showing that LinTT1 peptide molecules is present on liposomal surface and this amount of peptide can provide a specific targeting of resulting nanosystems *versus* biological models (Simón-Gracia et al., 2018b). These values were obtained starting from a liposomal concentration of 1.29×10^{12} nanovesicles/mL, and the final amount of conjugated LinTT1peptide (5.7×10^{16} peptide molecules/mL of final formulation) as reported in the Supplementary materials (Figure S1).

The conjugation between LinTT1 and DSPE-PEG2000mal by sulfhydryl-maleimide reaction caused the synthesis of DSPE-PEG2000-LinTT1. The reaction between maleimide group of DSPE-PEG2000 and sulfhydryl of LinTT1 form a stable synthetic derivative. The synthesis success was confirmed by ^{1}H NMR spectra of LinTT1, DSPE-PEGmal and DSPE-PEG2000-LinTT1. ^{1}H NMR of LinTT1, DSPE-PEG2000mal and DSPE-PEGmal-LinTT1 showed that the characteristic maleimide sharp peak at 7 ppm was present in the spectrum of DSPE-PEG2000mal, but not in that of DSPE-PEG2000-LinTT1, confirming the happened reaction (Figure S4). These results agree with data previously reported for a similar reaction process (Wang et al, 2019).

DOX, alone or in combination with SRF, was loaded in LinTT1-Lipo and tested *in vitro*, as described subsequently. Physicochemical characterization of therapeutic liposomes demonstrated that the hydrodynamic diameter of DOX-loaded liposomes (alone or in association with SRF) increased around 10 nm in comparison with empty ones, however no significant changes were found for the PDI and zeta-potential values (Table S1). Similar values of zeta-potential of empty and drugs-loaded nanovesicles demonstrated that DOX and SRF were entrapped inside the aqueous core and in the phospholipid bilayer of liposomes, respectively, and they were not adsorbed on nanovesicles' surface. The slight increase of average sizes of DOX-loaded liposomes can be ascribed to the DOX crystallization in the aqueous core of liposomes, as previously reported (Pasut et al., 2015). TEM analysis showed that liposomes have spherical-like shapes and their shape is not modified by the conjugation of LinTT1 on the surface of nanocarriers (Figures S2 and S3). All drug-loaded liposomes, both functionalized and bare ones, exhibited the physicochemical characteristics suitable for their systemic use as drug delivery systems for anticancer therapy: (i) an average diameter below than 200 nm suggesting their ability to penetrate intact through fenestrated vasculature of neo-formed tumor vessels and accumulate in tumor tissue (Maruyama, 2011; Blanco et al., 2015); (ii) a net negative charge suggesting colloidal stability of nanosuspension (Di Francesco et al., 2017a,b); and (iii) a PDI below than 0.2 showing a narrow size distribution of nanovesicles (Vakili-Ghartavol et al., 2020)

3.2. Hemocompatibility test

Erythrocytes are the main cells in the bloodstream and closely interact with nanomedicines after their intravenous injections (Pretini et al., 2019), suggesting that the hemocompatibility of a potential systemic nanoparticle needs to be investigated during the early stages of its development (de la Harpe et al., 2019). In this scenario, the hemocompatibility of LinTT1-Lipo was investigated and their incubation with human RBCs demonstrated that the conjugation of LinTT1 peptide on the surface of liposomes via PEG does not lead to a hemolytic nanosystem. LinTT1-Lipo induced a hemolysis percentage below than 2% for all tested lipid concentrations up to 48 h of incubation (Fig. 2), which is lower than the threshold of 5% fixed by ISO/TR 7405–1984 for hemolytic samples (Zhang et al., 2018). Results demonstrated that LinTT1-Lipo are safe and biocompatible and do not cause hemolysis of human RBCs, suggesting their suitable use for intravenous administration.

3.3. Drugs loading and in vitro release kinetic profiles of payloads

Multidrug liposomes were obtained by co-loading of SRF and DOX inside the liposomes based on their physicochemical properties and solubility (Xiao et al., 2016; Cai et al., 2014), and the relative entrapment efficiency (E.E.%) and drug loading (L.D.%) were evaluated using the proper calibration curve Equations (Figure S5). SRF, which is co-loaded in the bilayer of therapeutic liposomes, did not affect the high E.E. of DOX in the aqueous compartment. DOX-loaded liposomes, with

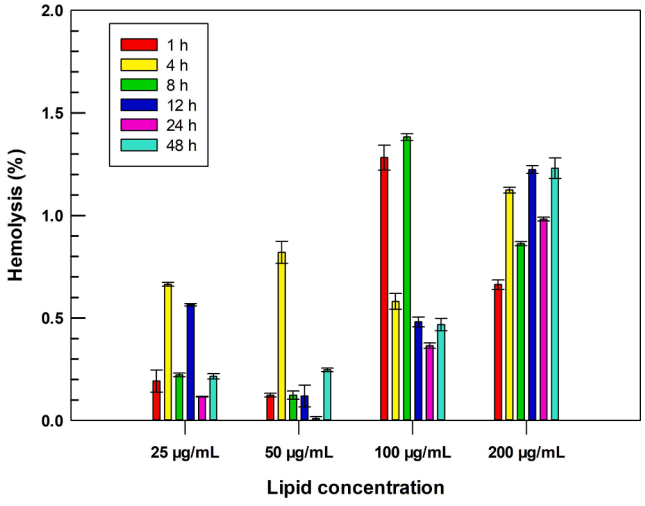

Fig. 2. Hemocompatibility of LinTT1-functionalized liposomes. Hemolysis was monitored up to 48 h of incubation with human erythrocytes at 37 °C. Different lipid concentrations (25, 50, 100, and 200 µg mL^{-1}) were tested during the analysis. Lysed hemoglobin was quantified in the supernatant at the wavelength of 577 nm using a UV–Vis spectrophotometer. Results are the average of three independent analysis ± S.D.

or without SRF, showed an E.E. of around 90% and a L.D. of 4.5% (Table S1). High E.E. of DOX inside the therapeutic liposomes depended on the crystallized drug that precipitates inside the aqueous core of liposomes, thus forming a gel-like structure as a consequence of transmembrane pH gradient and remote loading procedures that were used for the liposomes' preparation (Cheung and Al-Jamal, 2019; Fritze et al., 2006). Conversely, the E.E. and L.D. efficiencies of SRF-loaded liposomes were around 50% and 1.25%, respectively (Table S1). In particular, the co-loading of both drugs into the LinTT1-Lipo resulted in a slight reduction of E.E. of SRF from 51.6 ± 1.1 to 49.8 ± 0.4, while no-significant changes were observed for DOX (Table S1). These results were in agreement with data previously published for liposomes containing gemcitabine and paclitaxel in the same colloidal nanocarrier and the very slight decrease or the absence of significant changes in the drugs loading capacity could be explained by the different compartment localization of the two bioactive compounds (Cosco et al., 2011). Moreover, the entrapment and drug loading efficiencies for both drugs were very similar between bare-Lipo and LinTT1-Lipo, suggesting that the surface architecture of liposomes did not affect these parameters (Table S1).

The release kinetics of DOX and SRF from LinTT1-Lipo/D + S were evaluated into two different receptor media: PBS supplemented with FBS (10% v/v) and PBS supplemented with Tween 80 (Tw80) (1% v/v). The receptor media were chosen based on media previously reported elsewhere (Tahir et al., 2020; Guo et al., 2017) for the SRF release study. The analysis was performed at physiological pH and in acid condition (pH 5.5 and pH 6.5) in order to mimic the TME (Justus et al., 2013). Around 25% of DOX was released after 72 h of incubation in the medium supplemented with FBS and ≈30% of drug in the receptor medium supplemented with Tw80. No significant difference was observed for the cumulative release of DOX in the media that have different pH, thus having similar results after 72 h of incubation (Fig. 3). In particular, only slight differences were observed in the release profile of DOX after 3 h of incubation between physiological pH and pH = 5.5. These results demonstrated that the release kinetic of DOX from LinTT1-Lipo/D + S was independent of the pH of selected receptor media. This is in agreement with data previously reported elsewhere that demonstrated a similar kinetic release of DOX from PEGylated liposomes in PBS solution at pH 5.5 and 7.4 (Shibata et al., 2015). The lack of significant variations in the cumulative release of DOX at different tested pH-values could depend on the ammonium sulfate, and particularly the sulfate, used to generate the pH gradient during the remote loading procedures. In fact, sulfate is a base conjugate obtained after dissociation of strong acid, and the slight decrease of pH from 7.4 to only 5.5 does not allow its protonation, thus resulting in a massive interaction of negative sulfate with protonated DOX at specific pH range (from 5.5 to 7.4) used during the study as previously reported (Fritze et al., 2006). This property affects similar results obtained for the release kinetic of DOX at different pH-values (Fritze et al., 2006). Conversely, 10 ± 2% of SRF was released at pH 5.5 for both receptor media, while 12 ± 2% and 28 ± 4% of drug was released at pH 7.4 for receptor medium supplemented with FBS and Tw80, respectively (Fig. 3). Instead, the cumulative release of SRF at pH 6.5 was 17 ± 3% and 10 ± 1% in the medium supplemented with Tw80 and FBS, respectively, after 72 h of incubation.

Therefore, the release of SRF in the medium with Tw80 at pH 7.4 was twice that of the drug released in medium supplemented with FBS at the same pH (28 ± 4% for Tw80 versus 12 ± 2% for FBS). This difference needs more investigations, but probably the higher release of SRF in the receptor medium containing Tw 80 at pH 7.4 in comparison with pH 5.5 may depend on the lower critical micelle concentration (CMC) of this surfactant at physiological pH than the acid one, as previously demonstrated elsewhere (Bloor et al., 1970) for Tween 40 (Tw40) that have the same hydrophilic head of Tw80 and differs only for the acyl chain. This hypothesis is further supported by release data obtained at pH 6.5. Indeed, despite the SRF released in the medium supplemented with Tw80 is higher than that obtained for the medium supplemented with

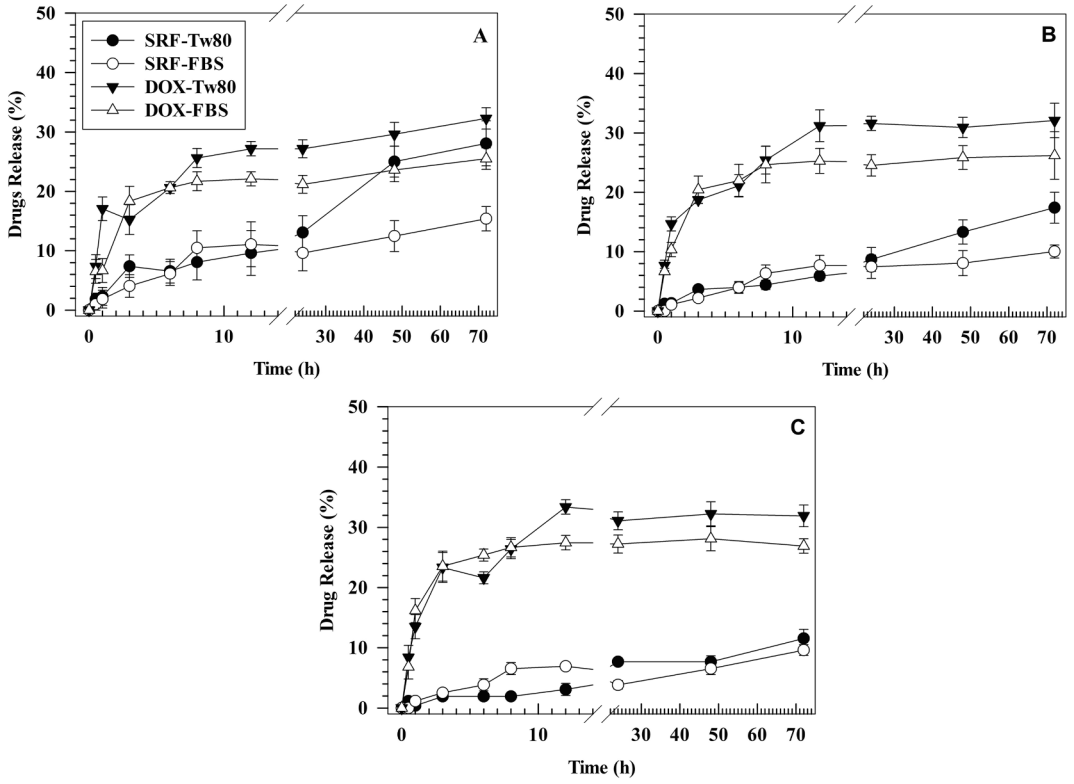

Fig. 3. Release kinetic of DOX and SRF from LinTT1-functionalized liposomes in two different media at pH 7.4 (A), pH 6.5 (B) and pH 5.5 (C), at 37 °C. The amount of released drugs was calculated by using external calibration curves as reported in Figure S7 and S8 of Supplementary material. Results are the average of three independent experiments ± S.D. Error bars, if not shown, are within symbols.

FBS after 72 h (17 ± 3% *vs.* 10 ± 1%, respectively), this difference was significantly lower than results obtained at physiological pH, thus showing that pH-value can affect the SRF release kinetic of LinTT1-liposomes in the accepting medium supplemented with Tw80.

Moreover, Tw80 is a non-ionic surfactant that can be adsorbed on the external surface of liposomal bilayer, thus making mixed micelles with lipids of liposomes, as previously reported for other lipids (Paolino et al., 2017). This complex can favor strong interaction between Tw80 and SRF diffused across lipid bilayer resulting in the leakage of liposomes supramolecular structure. This may increase the solubility of SRF and its release in the medium supplemented with Tw80, especially at pH 7.4, where the lower CMC of this surfactant improves its solubilizing properties.

Release kinetic of SRF and DOX in different experimental conditions have a biphasic release kinetic with rapid and continuous release following a zero-order kinetic up to 12 h of incubation, and a plateau from 24 to 72 h of incubation (Fig. 3). Results showed that LinTT1-Lipo were able to co-deliver continuously DOX and SRF up to 72 h in physiological and acid media without a massive and rapid release of payloads. These findings showed a sustained drugs release from functionalized liposomes, suggesting the ability of this nanosystem to avoid the rapid cargo leakage, thus potentially reducing the side effects of delivered chemotherapeutic agents (Bozzuto and Molinari, 2015). In particular, DOX crystallization hampered the quick leakage of drug after *in vitro* and *in vivo* use and significantly increased the encapsulation efficiency of doxorubicin hydrochloride in the aqueous core of liposomes. This is a direct effect of drug-gel-like structure occurred in the aqueous core of liposomes using pH-gradient and remote procedure as previously reported for Doxil/Caelyx (Barenholz, 2012) and depend on different physicochemical parameters that are specific for drug candidates (Cern et al., 2014; Cern et al., 2017).

However, the gel-like structure resulted by crystallizing doxorubicin hydrochloride and the resulting slow and constant drug release did not affect and/or decrease the anticancer efficacy of payload and its cytotoxicity on breast cancer cells. In fact, LinTT1-liposomes can be targeted from breast cancer cells overexpressing LinTT1 specific receptors and colloidal nanocarriers were like a depot system, which favored the accumulation of crystallized doxorubicin hydrochloride inside the cancer cells and provided the slow dissolution of payload in the intracellular compartment, as reported elsewhere (Li et al., 2019; Wei et al., 2015).

Based on these, the therapeutic effects of drugs were not compromised *in vivo* due to the biodegradable properties of liposomes that are degraded after internalization in tumor tissues and then release payloads (Costanzo et al., 2019).

3.4. Stability studies in human plasma

Nanomedicines should remain stable after systemic injection and biomaterials making polymeric shell or lipid bilayer were selected to protect nanocarriers from destabilization phenomenon occurring after interaction with plasma proteins (Immordino et al., 2006). Nanocarriers injected *in vivo* interact with circulating cells and proteins and these phenomena may cause several mechanical stresses and activate enzymatic processes (Di Francesco et al, 2021). These drawbacks can strongly decrease the therapeutic effect of nanomedicines, thus causing degradation of nanocarriers, with the quick leakage of payloads, or their rapid clearance from bloodstream and significant macrophage uptake (Ferrari, 2010). Circulating serum proteins play a crucial role for the potential modification of surface properties in nanocarriers, and thus, their destabilization after systemic injection (Pasut et al., 2015), due to protein corona phenomenon (Palchetti et al., 2016). Protein corona significantly modifies the physicochemical properties of nanocarriers, thus increasing average sizes and size distribution, as well as their surface properties and compositions (Hadjidemetriou et al., 2019). Protein corona phenomenon can also facilitate the macrophage uptake of nanocarriers, and thus, their clearance through the reticuloendothelial system (RES) organs (Monopoli et al., 2012). In these attempts, we studied the stability of LinTT1-lipo + D/S after incubation with human plasma and the resulting data was compared that obtained for Caelyx-like Lipo (control), which is similar to Doxil/Caelyx liposomal formulations currently approved from Food and Drug Administration and European Medicine Agency for the treatment of breast cancer (Monopoli et al., 2012, Bulbake et al., 2017). LinTT1-lipo + D/S and Caelyx-like Lipo had similar trend for average sizes after 72 h of incubation in human plasma (Fig. 4). They showed a slight decrease of particle sizes (~15 nm) in the 1 h of incubation, maybe due to the adsorption of a weak protein corona on the surface of PEGylated liposomes. This process resulted in an osmotic gradient on liposomal surface leading to the shrinkage of nanocarriers, and thus, the leakage of water content from the aqueous core of liposomes (Wolfram et al., 2014b). Conversely, the average sizes of LinTT1-lipo + D/S and Caelyx-like Lipo increased after 48 h of incubation and this phenomenon increased significantly after 72 h of incubation with resulting average sizes of ~ 230 nm and ~ 180 nm for LinTT1-Lipo + D/S and Caelyx-like Lipo (Fig. 4), respectively. The significant increase of particle sizes at 48 and 72 h of incubation, may depend on a biphasic process occurring during the formation of protein corona on nanocarriers surface. In fact, we can hypothesize that during the early stages of incubation, proteins having high concentrations but low affinity for liposomal bilayer, formed an unstable protein corona, which is in equilibrium and exchanges with the surface of liposomes without changing significantly particle sizes. Conversely, at long incubation times (48 and 72 h), circulating proteins, making protein corona, had a low concentration but high affinity for liposomes. The high affinity protein corona for liposomal surface replaced soft corona, adsorbed at short incubation times, with hard corona that stack to the surface of nanocarriers and thus increased their average size (Pozzi et al., 2015; Wolfram et al., 2014b). The resulting data also demonstrated that LinTT1-lipo + D/S and Caelyx-like Lipo were stable and did not change their average sizes up to 24 h (Fig. 4). The stability tests supported our hypothesis that LinTT1-Lipo + D/S is stable in human plasma and circulating proteins do not affect nanocarrier stability, and fostered a potential *in vivo* translation of LinTT1-Lipo + D/S.

Despite, the significant increment of particle size after 72 h of incubation with human plasma, average sizes of Caelix-like Lipo and LinTT1-Lipo + D/S were less than twice compared to the initial data (~112 nm (Caelix-like Lipo) and ~ 160 nm (LinTT1-Lipo + D/S) at time point 0 *vs.* ~ 180 nm (Caelix-like Lipo) and ~ 230 nm (LinTT1-Lipo + D/S) at 72 h), thus supporting the hypothesis that nanocarriers did not make aggregates after 72 h of incubation in human plasma, but the

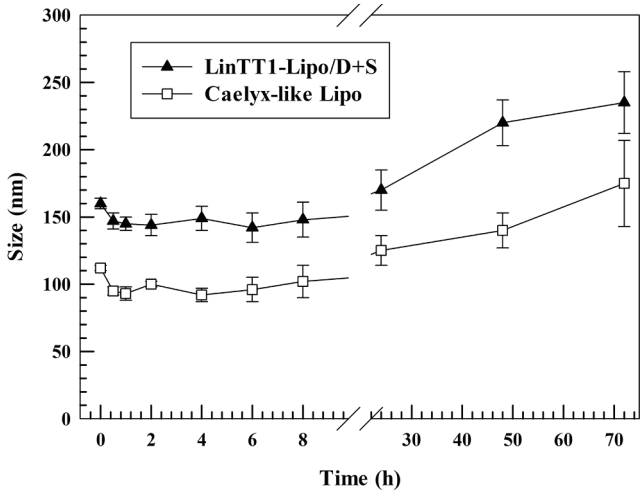

Fig. 4. Human plasma stability of LinTT1-Lipo + D/S and Caelyx-like Lipo. Results are the average of three independent experiments ± S.D. (n = 3). Error bars, if not shown, are within symbols.

increase of sizes depended on the resulting protein corona adsorbed on the surface of liposomes (Pozzi et al., 2015; Wolfram et al., 2014b). Our hypothesis was further supported by Turbiscan analysis, which demonstrated the lack of aggregation for LinTT1-Lipo + D/S and Caelix-like Lipo in saline solution (NaCl) 0.9%, w/v, (Figure S9) and medium (saline solution NaCl 0.9%/human plasma, 50:50 (v/v)) (Figure S10) at 37 °C. LinTT1-Lipo + D/S and Caelix-like Lipo had BS and T signal variations below 5% and 10% during the incubation time (1 h) and their relative lines were overlapped with the threshold baseline (Di Francesco et al., 2017a,b). The presence of negative or positive peak variations for BS and T signals at samples height over 8 mm and below 2 mm did not depend on the nanocarrier destabilization but was related to air bubbles present at the interfaces on the top or bottom of glass holder during the analysis (Celia et al., 2009). The long-term stability of LinTT1-Lipo + D/S and Caelix-like Lipo in human plasma were further confirmed by destabilization kinetic profiles which were similar for both nanocarriers (Figure S11). These results were in agreement with data herein reported for DLS analysis (Fig. 4), and thus, demonstrate that LinTT1-Lipo + D/S is stable and has suitable physicochemical properties for a potential injection in the bloodstream.

3.5. *In vitro cytotoxic effect on 2D cell models*

DOX, as a free drug or formulated as PEGylated liposomes, is currently one of the most used chemotherapeutic drugs to treat breast cancers, and particularly TNB cancer (Waks and Winer, 2019). DOX is usually administereted in combination with other cytotoxic drugs, such as paclitaxel and cyclophosphamide (Waks and Winer, 2019; Tampaki et al., 2018), and these combinations have a synergistic effect that results in a decreased effective dosage of drugs compared to mono-therapy (Fisusi and Akala, 2019). This approach decreases the side effects and modifies the induction rate of cancer resistant phenomena (Waks and Winer, 2019; Yardley, 2013). Despite controversial results about the use of SRF in combination with other chemotherapeutic agents in breast cancer therapies, some clinical trials are still ongoing (Chen et al., 2019a; Hwang et al., 2019). Moreover, several animal investigations have clearly shown the ability of SRF to increase the anticancer properties of chemotherapic agents commonly used in clinic for breast cancer therapies, especially when the two drugs were co-loaded in the same nanocarriers. In these attempts, Sui et al. recently demonstrated the higher anticancer efficacy of SRF-loaded into pullulan-DOX conjugated nanoparticle than the same nanosystem containing only DOX, on murine breast cancer carcinoma (Sui et al., 2017). In this study, they also showed a great reduction of side effects when the two drugs were co-loaded into nanoparticles than the combination of free drugs administered in the free form. Similar results were also observed by Lei et al., which demonstrated a great synergistic effect of SRF and paclitaxel when the two drugs were co-loaded into the same liposomal carrier, on MCF-7/multidrug resistant cancer in mice (Lei et al., 2019).

In our study, the capability of SRF to potentiate the cytotoxic effect of DOX was tested in two different breast cancer cell lines. In particular, a positive estrogen receptor (MCF-7) and a triple negative (MDA-MB-231) breast cancer cell lines were used during the study. The cytotoxic effect was evaluated based on drug concentrations (0.01–10 μM) and incubation times (24, 48 and 72 h). Drug concentration, for the *in vitro* tests, is reported as a ratio to the DOX concentration, which is three-fold higher than SRF at different incubation time points. This difference depends on the final concentration of DOX and SRF, which are co-loaded inside liposomes, being 1600 and 540 μM for DOX and SRF, respectively. As the first step, the cytotoxic effect of DOX as a single agent was compared with the cytotoxic effect provided by the association of SRF and DOX, both in free form or loaded in bare liposomes (Fig. 5). The cytotoxic effect of SRF as a single agent was not investigated in this study, because despite its potential ability to increase the efficacy of breast cancer therapies when it is co-administered with other chemotherapeutics, its efficacy as single agent has been demonstrated to be poor in breast cancer (Bronte et al., 2017).

SRF significantly increased the cytotoxic effects of DOX when the two drugs were co-loaded in bare liposomes in positive estrogen receptors (MCF-7) and in TNB cancer (MDA-MB-231) cell lines, compared to free drugs (Fig. 5).

This effect was similar in MCF-7 and MDA-MB-231 cells. In particular, after 24 h of incubation, the cytotoxic effect of free DOX and combined free DOX and SRF was very similar for all drug concentrations in both investigated cell lines. On the contrary, at the same incubation time point, the cytotoxic effect of DOX and SRF co-loaded in bare liposomes (bare-Lipo/D + S) was significantly higher than bare liposomes containing only DOX (bare-Lipo/D), at the DOX concentration of 0.5 and 1 μM, and SRF concentration equivalent to 0.17 and 0.35 μM, respectively. The ability of SRF to improve the cytotoxic effect of DOX when the two drugs were co-loaded in bare liposomes in comparison with free drugs, became more evident after 48 and 72 h of incubation (Fig. 5). After 48 h of incubation, bare-Lipo/D + S showed a cell death of 45.8 ± 2.9% and 60.0 ± 3.6% on MCF-7 cell line at the DOX concentration of 0.5 μM (and SRF concentration equivalent to 0.17 μM) and at DOX concentration of 1 μM (and SRF concentration equivalent to 0.35 μM), respectively; while bare-Lipo/D demonstrated a cell death of 32.2 ± 4.5% and 44.3 ± 3.1% at the same DOX concentrations, respectively. Furthermore, the association of free drugs resulted in a slight reduction of cell viability compared with free DOX. After 48 h of incubation, MCF-7 cells showed a cell death of 27.7 ± 4.9% and 38.3 ± 3.6% when treated with combined drugs at DOX concentration of 0.5 μM (and SRF concentration equivalent to 0.17 μM) and at DOX concentration of 1 μM (and SRF concentration equivalent to 0.35 μM), respectively; and 22.5 ± 2.9% and 30.6 ± 4.8% for free DOX as single agent at the same DOX concentrations, respectively. Similar trend was observed in MDA-MB-231 cells after 48 h of incubation with bare-Lipo/D, showing a cell death of 44.5 ± 2.1% at DOX concentration of 0.5 μM, while cell treated with bare-Lipo/D + S showed a cell death of 58.1 ± 4.4% at the same DOX concentration and SRF equivalent concentration of 0.17 μM. Also, in this cell line, the cytotoxic synergistic effect of combined free drugs was lower than DOX and SRF co-loaded liposomes. Indeed, after 48 h of incubation, the cell death was 32.8 ± 5.9% at DOX concentration of 0.5 and 39.9 ± 6.3% at the same DOX concentration (and SRF concentration equivalent to 0.17 μM), for free DOX and combined free drugs, respectively.

Moreover, after 72 h of incubation with bare-Lipo/D + S the cell death was of 59.2 ± 5.9% and 74.2 ± 4.6% at DOX concentration of 0.5 μM (and SRF concentration equivalent to 0.17 μM), for MCF-7 and MDA-MB-231 cell line, respectively (Fig. 5). Conversely, combinations of free drugs had a similar cytotoxic effect herein reported (61.5 ± 3.6% and 68.2 ± 5.2%) at DOX concentration equivalent to 1 μM (and SRF concentration equivalent to 0.35 μM), for MCF-7 and MDA-MB-231 cell lines, respectively (Fig. 5). This effect highlighted the potentiality of liposomes to decrease the therapeutic drugs dosage for efficacious treatment in breast cancer (Meng et al., 2016).

The increased cytotoxic efficacy of bare-Lipo/D + S in comparison with the association of free drugs was probably due to the enhanced synergistic effect of the two chemotherapeutic drugs in response to their allocation in the same nanovesicle, which provided an increased uptake from breast cancer cells and reduced destabilization phenomena on drugs molecules (Sercombe et al., 2015). Based on these findings, for further analysis concerning the cytotoxic efficacy, liposomes containing both drugs were used. The cytotoxic effect of DOX and SRF, as free drugs or formulated as liposomes, was always higher in MDA-MB-231 cells than MCF-7 cells. This difference depends on the higher responsiveness of MDA-MB-231 cells than MCF-7 ones to DOX (Lovitt et al., 2018).

One of the main challenges in anticancer therapies is to target specifically the pathological tissues, improving the efficacy of therapy and decreasing side effects on healthy cells (Yan et al., 2020; Pu et al., 2019). In these attempts, we functionalized liposomes by conjugating onto the surface of liposomes via PEG the LinTT1 peptide, a specific ligand for

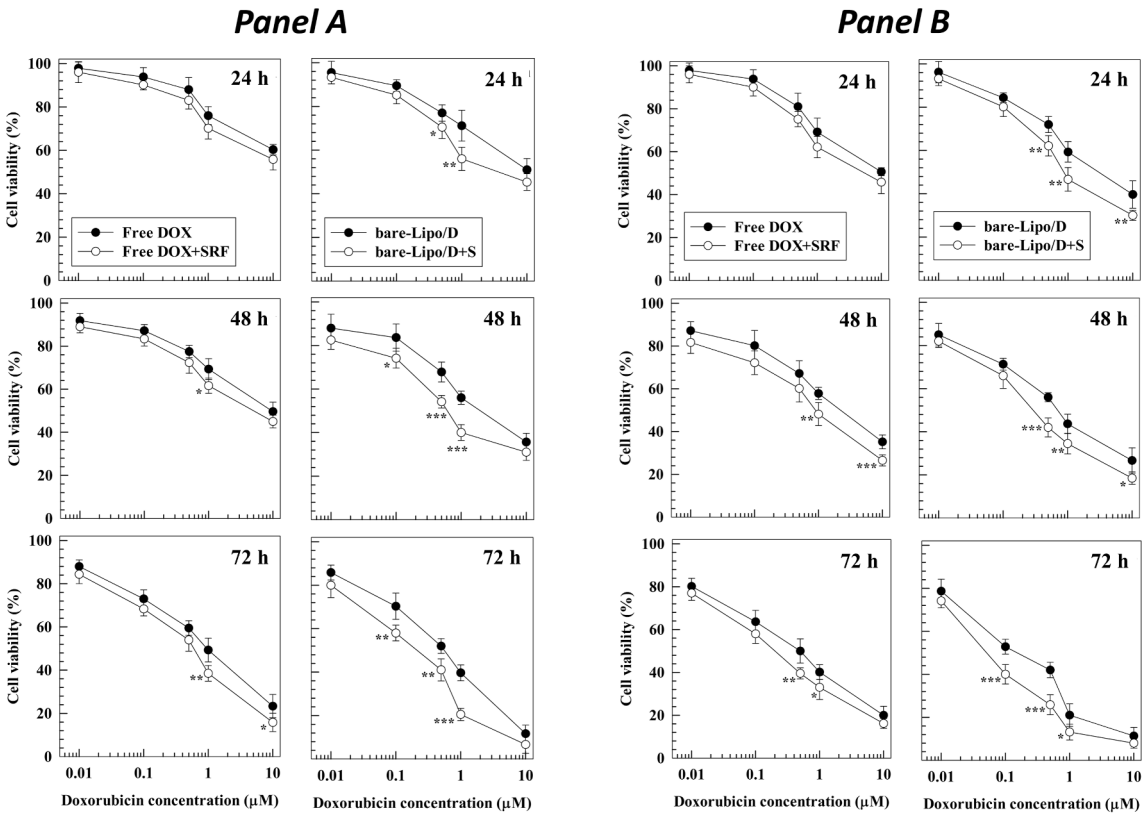

Fig. 5. *In vitro* cytotoxic activity of DOX, as single agent or combined with SRF, in free form or loaded into liposomes on MCF-7 (Panel A) and MDA-MB-231 (Panel B) cell lines using a 2D breast cell culture model. Cytotoxic effect was reported as cell viability percentage (%) and evaluated as a function of incubation times and drug concentrations. Cellular viability percentage (%) was evaluated by using CellTiter-Glo luminescence assay. Results are the average of at least three independent experiments ± S.D. Statistical significance was set at: *p < 0.05, **p < 0.01, and ***p < 0.001. Cell viability (%) of cells treated with empty liposomes was always over than 90% for all tested concentration and incubation time points (data not shown). Error bars, if not shown, are within symbols.

p32 receptor that is overexpressed on cytoplasmic membrane by several breast cancer cell lines (Fogal et al., 2008; Simón-Gracia et al., 2018b). The cytotoxic effect of LinTT1-Lipo/D + S liposomes was evaluated *in vitro* using MCF-7 cells and MDA-MB-231 cells. The anticancer activity of LinTT1-Lipo/D + S was compared to bare-Lipo/D + S (Fig. 6). LinTT1-Lipo/D + S increased the cytotoxic effect of payloads on MCF-7 cells and MDA-MB-231 cells compared to bare-Lipo/D + S (Fig. 6).

In particular, the conjugation of LinTT1 onto the surface of therapeutic liposomes increased significantly the anticancer activity in 2D cell models of MCF-7 and MDA-MB-231 breast cancer cells at shorter incubation time (24 h) than longer ones (48 and 72 h) (Fig. 6). These differences may depend on the static experimental conditions of the analysis that forced the interactions between liposomes and cells and the resulting uptake of nanovesicles, thus suppressing or greatly reducing differences between LinTT1-Lipo/D + S and bare-Lipo/D + S at long incubation times. This phenomenon does not reflect the physiological conditions occurring *in vivo*, where "washing properties" of blood stream and the solid cancer 3D architecture decrease the contact between nanoparticles and cell surface (Palange et al., 2014).

The cell death percentage (%) at DOX concentration of 0.1 μM and SRF corresponding concentration of 0.035 μM was 14.8 ± 4.0% and 29.2 ± 3.6%, respectively, for bare-Lipo/D + S and LinTT1-Lipo/D + S after 24 h of incubation on MCF-7 cells (Fig. 6A). Similar results were also obtained for MDA-MB-231 cells, where LinTT1-Lipo/D + S had a cell death percentage (%) of 40.1 ± 3.7% compared to bare-Lipo/D + S (19.8 ± 4.4%) after 24 h of incubation, at the same drug concentrations (Fig. 6B). Moreover, LinTT1-Lipo/D + S provided a higher cell death than bare-Lipo/D + S for all drug concentrations investigated after 24 h of incubation, on both cell lines (Fig. 6). Furthermore, less significant (or no significant) differences were observed between LinTT1-Lipo/D + S and bare-Lipo/D + S after 48 and 72 h of incubation. At the DOX concentration of 0.1 μM and SRF corresponding concentration of 0.035 μM, the cell viability of MCF-7 cells was 70.2 ± 4.6% and 64.8 ± 4.0% when treated with bare-Lipo/D + S and LinTT1-Lipo/D + S, respectively, after 48 h of incubation. Significant differences between the two formulations were observed in this cell line only at DOX concentration of 0.5 μM and SRF corresponding concentration of 0.17 μM, and at DOX concentration of 10 μM and SRF corresponding concentration of 3.5 μM, after 48 h of incubation. These differences were still significantly lower than the ones observed on the same cell line at the same drugs concentration after 24 h of incubation. Similar trend was observed after 72 h of incubation, where only at the two lowest drugs concentration significant differences were found between bare-Lipo/D + S and LinTT1-Lipo/D + S, on MCF-7 cells. In particular, at DOX concentration of 0.01 μM and SRF corresponding concentration of 0.0035 μM, this cell line showed a cell viability of 79.6 ± 5.6% and 70.4 ± 3.2%, for bare-Lipo/D + S and LinTT1-Lipo/D + S, respectively, after 72 h of incubation; while it showed a cell viability of 58.1 ± 3.4% and 51.3 ± 4.0% for bare-Lipo/D + S and LinTT1-Lipo/D + S, respectively, at the DOX concentration of 0.1 μM and SRF corresponding concentration of 0.035 μM, at the same incubation time point. Similar results were obtained on MDA-MB-231 cells that demonstrated less significant (or no-significant) differences of cell viability between bare-Lipo/D + S and LinTT1-Lipo/D + S for almost all drugs concentrations after 48 and 72 h, compared to 24 h of incubation. Moreover, in this cell line, LinTT1-Lipo/D + S provided a higher cytotoxic efficacy than bare-Lipo/D + S only at DOX concentration of 0.01, 0.1 and 1 μM and SRF corresponding concentration of 0.0035, 0.035 and 0.35 μM, respectively, after 48 h of incubation; and at DOX concentration of 0.01, 0.1 μM and SRF corresponding concentration of 0.0035, 0.035, respectively, after 72 h of incubation. When

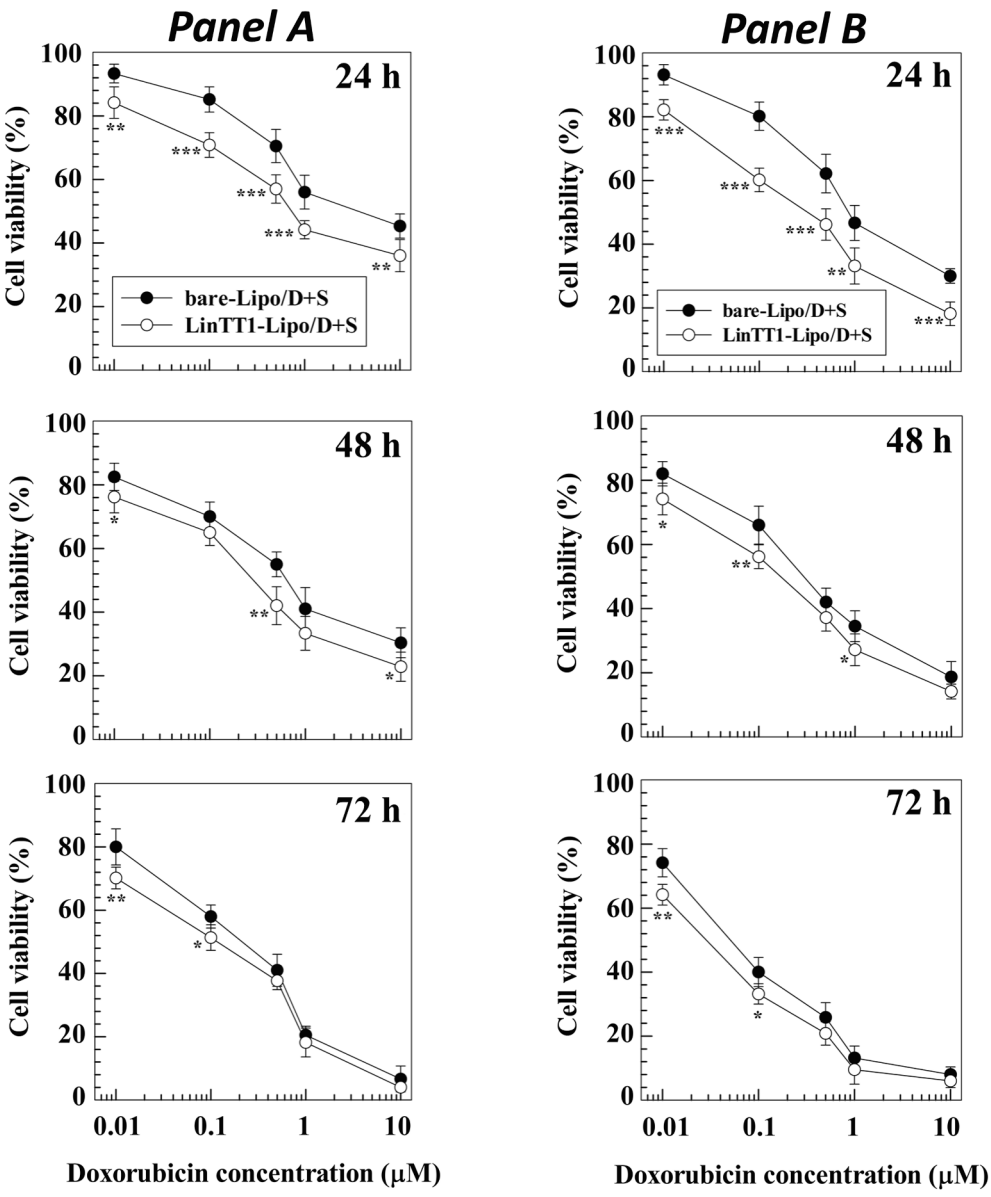

Fig. 6. *In vitro* cytotoxic activity of DOX and SRF, co-loaded LinTT1-functionalized liposomes on MCF-7 (Panel A) and MDA-MB-231 (Panel B) cell lines using 2D breast cancer cell models. Cytotoxic effect was reported as cell viability percentage (%) and evaluated as a function of incubation times and drug concentrations. Cell viability percentage (%) of therapeutic LinTT1-functionalized liposomes was compared to therapeutic bare liposomes. Cellular viability percentage (%) was evaluated by using CellTiter-Glo luminescence assay. Cells treated with cell culture medium are the control and correspond to 100% of cell viability for all tested concentrations at different times of incubation. Cells treated with empty LinTT1-Lipo demonstrated a cell viability over 90% for all tested concentrations (data not shown). Results are the average of three independent experiments ± S.D. Statistical significance was set at: *$p < 0.05$, **$p < 0.01$, and ***$p < 0.001$. Error bars, if not shown, are within symbols.

significant, the differences between bare-Lipo/D + S and LinTT1-Lipo/D + S after 48 and 72 h of incubation were still less significant than the ones observed after 24 h of incubation at the same drugs concentrations. These results demonstrate that the functionalization of the liposomes' surface with LinTT1 peptide increased the cytotoxic effect of therapeutic liposomes on MCF-7 and MDA-MB-231 breast cancer cell lines compared to bare therapeutic liposomes, especially after low incubation time point. These findings suggest that the conjugation of this ligand on therapeutic liposomes' surface promoted the interaction rate and cellular uptake of nanovesicles on both investigated cell lines.

3.6. *In vitro cytotoxic effect on 3D spheroid cell models*

3D spheroids of breast cancer cells were created to simulate *in vivo* nanoparticle distributions and uptake in tumor tissues. 3D spheroid breast cancer cellular model was obtained using a TNB cancer cell line (MDA-MB-231 cells). TNB cancer is currently a priority in breast cancer therapy due to its decreased responsiveness to the current endocrine and targeted therapies. TNB cancer cells are mutated and lack of physiological pathways like progesterone receptors (PR), estrogen receptors (ER) and human epidermal growth factor receptor 2 (HER2), being non-responsive to the treatment that targets these receptors (Lee and Djamgoz, 2018). In these attempts, estrogen-receptor positive breast cancer is currently well treated with hormonal therapies and have a 5-year breast cancer–survival of 99% at the stage I (tumor mass smaller than 2 cm without the involvement of lymph node), while estrogen receptor metastatic cancer has a median overall survival of 4–5 years. Conversely, TNB cancer has a poorer prognosis showing a 5-year breast cancer–survival of 85% at the stage I and a median overall survival of 10–13 months for metastatic phenotype (Waks and Winer, 2019; Chavez-MacGregor et al., 2017). These findings highlight the urgent priority to develop new therapies for TNB cancer that lacks targeted therapies in contrast to PR, ER and/or HER2 positive breast cancer (Al-Mahmood et al., 2018). For these reasons, the efforts in breast cancer research are mainly focused on TNB cancer and in line with this statement we decided to focus our work in the study of TNB 3D cancer cell models.

Human fibroblast (20% of total cells) were used to stabilize the 3D structure of MDA-MB-231-based spheroids (Rustamov et al., 2019), thus providing also a better correspondence with *in vivo* pathological conditions, where fibroblasts strongly affect the tumor proliferation (Kalluri and Zeisberg, 2006; Sahai et al., 2020). The cytotoxic activity of LinTT1-Lipo/D + S, bare-Lipo/D + S and the association of free DOX and SRF

was evaluated in 3D spheroids of MDA-MB-231 cells and the differences for cell viability (%) among the treatments were obtained (Fig. 7). We have previously demonstrated that bare-Lipo/D + S and LinTT1-Lipo/D + S increased the cytotoxic effect of combined payloads compared to the native drugs in 2D of breast cancer cells (Figs. 5 and 6). These results were similar in 3D spheroids where the cytotoxic effect of both bare-Lipo/D + S and LinTT1-Lipo/D + S was higher than the combination of two drugs in the free form for the MDA-MB-231 cells (Fig. 7). Conversely to 2D cell results, the cytotoxic effect of LinTT1-Lipo/D + S was higher than bare-Lipo/D + S for almost all tested incubation times and concentrations, in the 3D spheroids of MDA-MB-231 cells. Here, the cytotoxic effect of LinTT1-Lipo/D + S was higher than bare-Lipo/D + S from the lowest incubation time point (6 h) and these differences became more evident at long incubation time points, also at low drugs concentrations (Fig. 7).

The cell viability was 66.7 ± 4.6% and 77.2 ± 3.7% for LinTT1-Lipo/D + S and bare-Lipo/D + S, respectively, after 24 h of incubation at the DOX concentration of 0.5 μM and SRF corresponding concentration of 0.17 μM.

Similar differences were observed between the two formulations after 48 and 72 h of incubation. After 48 h of incubation the cell viability was 50.8 ± 4.9% and 65.4 ± 7.1% for LinTT1-Lipo/D + S and bare-Lipo/D + S, respectively, at the DOX concentration of 0.5 μM and SRF corresponding concentration of 0.17 μM. A significant difference was also observed between the two formulations at the same incubation time point at the DOX concentration of 1 μM and SRF corresponding concentration of 0.35 μM, where the cell viability was 44.2 ± 3.6% and 58.6 ± 6.8% for LinTT1-Lipo/D + S and bare-Lipo/D + S, respectively. After 72 h of incubation the difference between LinTT1-Lipo/D + S and bare-Lipo/D + S were still significant at the DOX concentration of 0.5 μM and SRF corresponding concentration of 0.17 μM, showing a cell viability of 40.9 ± 4.1% and 56.4 ± 3.7%, respectively. Similar trend was found at the DOX concentration of 1 μM and SRF corresponding concentration of 0.35 μM where spheroids treated with LinTT1-Lipo/D + S and bare-Lipo/D + S had a viability of 31.7 ± 3.3% and 43.1 ± 4.8%, respectively, after 72 h of incubation. Moreover, at this incubation time point, LinTT1-Lipo/D + S showed a higher cytotoxic effect than bare-Lipo/D + S also at DOX concentration of 0.1 μM and SRF corresponding concentration of 0.035 μM, showing a cell viability of 54.4 ± 5.1% and 67.2 ± 3.9%, respectively. Conversely with results obtained for MDA-MB-231 2D cell model (Fig. 6B), in the 3D spheroids of MDA-MB-231 cells the data demonstrated an improved cytotoxic effect of LinTT1-Lipo/D + S compared to bare-Lipo/D + S also for long incubation time points (48 and 72 h) (Fig. 7).

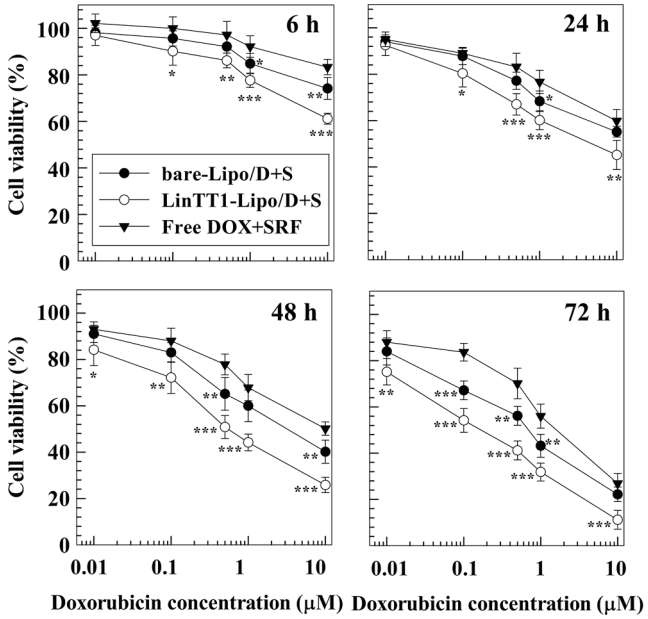

Fig. 7. *In vitro* cytotoxic activity of DOX and SRF free or co-loaded into bare- and LinTT1-functionalized liposomes in 3D spheroids of MDA-MB-231 cells. The cytotoxic activity was evaluated at different drug concentrations and incubation times. Results are reported as cellular viability percentage (%) and were obtained by using RealTime-Glo MT Cell Viability Assay. Data is the average of three independent experiments ± S.D. Control is 3D spheroids of MDA-MB-231 cells that are treated with cell culture medium and corresponds to 100% of cell viability for all tested concentrations at different times of incubation (6, 24, 48 and 72 h). Spheroids treated with empty LinTT1-Lipo and empty bare-Lipo demonstrated a cell viability over 90% for all tested concentrations (data not shown). Differences were evaluated between cytotoxic effects of combined free DOX and SRF and drugs co-loaded liposomes (both bare and functionalized ones). Statistical significance was set at: *$p < 0.05$, **$p < 0.01$, and ***$p < 0.001$. Error bars, if not shown, are within symbols.

This difference may depend on both, the "non-realistic interaction" between cancer cells in the 2D cell model that provided a higher uptake of nanoparticles (Behzadi et al., 2018), resulting in the lack of differences between functionalized and bare liposomes after long incubation time points, and also the hypoxic condition in the core of 3D spheroids that increased the overexpression of p32 protein receptors on breast cancer cell surface (Fogal et al., 2008; Song et al., 2019; Paasonen et al., 2016). Moreover, results demonstrated that higher concentrations of chemotherapeutic agents were required in the 3D cell model in comparison to the 2D cell model in order to provide a similar cytotoxic effect. These results are in agreement with data previously reports for other chemotherapeutic drugs that are used in similar 3D spheroids of breast cancer model (Figueiredo et al., 2019), and depended on the higher proliferation of breast cancer cells in the 2D model than the 3D spheroid model, thus resulting in an increased anticancer efficacy of payloads in MDA-MB-231 cells when cultured as mono-layer model (Frohlich, 2018).

3.7. 3D spheroids and interaction studies

Next, the internalization and uptake of LinTT1-Lipo was qualitatively and quantitatively evaluated in 3D spheroids of MDA-MB-231 cells with a diameter around 600 μm, using confocal laser scanning microscopy and flow cytometry, respectively (Fig. 8). The uptake of LinTT1-Lipo was evaluated at the incubation time points of 3 and 6 h, and was compared to the internalization of bare-Lipo. Positive events and the localization of the liposomes were evaluated through flow cytometry analysis and confocal laser scanning microscopy, respectively. For these studies, fluorescently labeled bare-Lipo were synthesized by adding a fluorescent lipid (DHPE-fluorescein, at 0.1% w/w) in the lipid bilayer during the preparation procedure, while LinTT1-Lipo resulted fluorescent thanks to the presence of fluorescent FAM molecule in the peptide backbone structure. Flow cytometry analysis and confocal analyses were carried out using only 3D spheroids of MDA-MB-231 cells to better mimic an *in vivo* situation (Behzadi et al., 2018).

Flow cytometry analysis demonstrated that LinTT1-Lipo were more taken-up and then significantly internalized by 3D spheroids of MDA-MB-231 cells than bare-Lipo, after 3 h of incubation. (Fig. 8A). The percentage of positive cells was 7.4 ± 2.1% and 25.3 ± 4.6% for bare-Lipo and LinTT1-Lipo (Fig. 8A), respectively.

Uptake and internalization of LinTT1-Lipo increased by increasing the incubation time up to 6 h (Fig. 8A). After 6 h of incubation time, the percentage of positive cells were 30.3 ± 4.3% and 40.2 ± 2.5% for bare-Lipo and LinTT1-Lipo (Fig. 8A), respectively, that is more than double for bare liposomes and almost double for LinTT1-Lipo. The fluorescence of bare- and LinTT1-Lipo associated to the cell membrane of MDA-MB-231 cells forming the 3D spheroids, which are not internalized, was quenched using a trypan blue solution. Results suggested that bare-Lipo and LinTT1-Lipo have different pathways of interaction with 3D the spheroid tumor model of MDA-MB-231 cells. The increased interaction of LinTT1-Lipo with cells in comparison with bare-Lipo depends on the

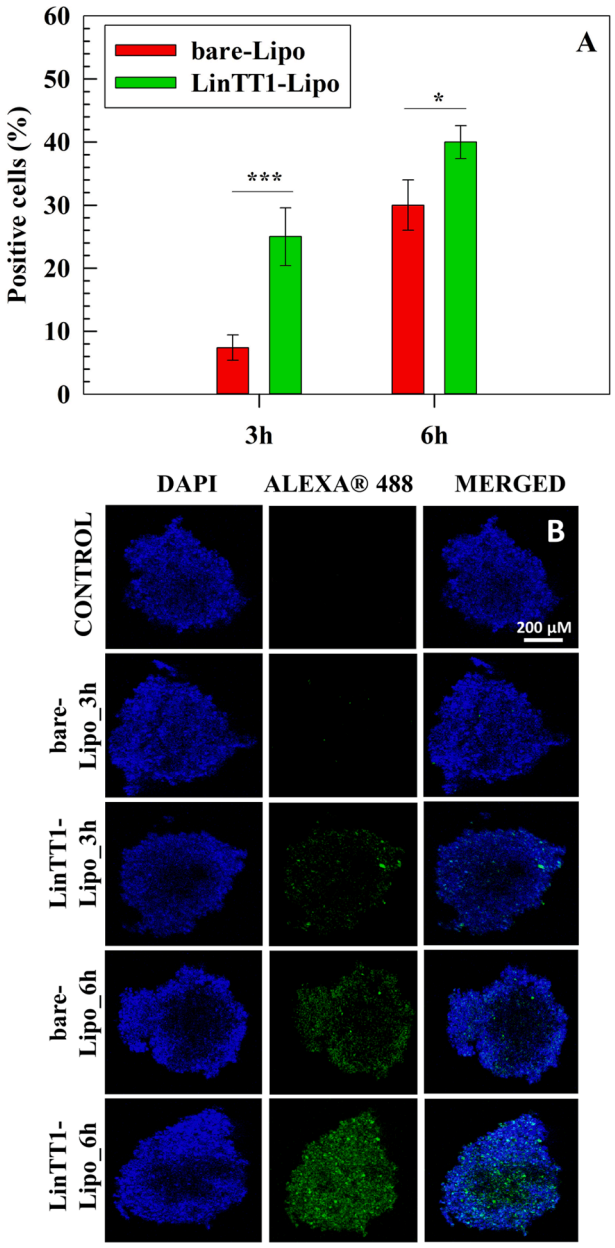

Fig. 8. *In vitro* interaction between bare- and LinTT1-funtionalized liposomes and 3D spheroids of MDA-MB-231 cells. The quantitative analysis of cellular uptake and internalization was evaluated by using flow cytometry analysis (A). 500 µg mL^{-1} of bare and LinTT1-functionalized liposomes were incubated with 3D spheroids of MDA-MB-231 cells at 37 °C for 3 and 6 h. The obtained data were normalized using the untreated cells as a control. Fluorescent positive cells were evaluated at the incubation time herein reported. At least 10,000 events were collected for each measurement. Qualitative analysis was obtained by using confocal laser scanning microscopy (B). DAPI (blue) was used to stain the nucleus, while Alexa Fluor 488 channel (green) was used to detect fluorescence of bare- and LinTT1-Lipo. The merged panels show the interaction between bare and LinTT1-Lipo with 3D spheroids of MDA-MB-231 cells. Scale bar is 200 µm. Results are the average of three independent experiments ± S.D. Statistical significance was set at: *$p < 0.05$, **$p < 0.01$, and ***$p < 0.001$.

presence of p32 receptor on cancer cells' membrane, as demonstrated for other LinTT1-functionalized nanoparticles through the pre-incubation of a blocking anti-p32 antibodies with cancer cells, that significantly inhibited the binding between cells and LinTT1-functionalized nanoparticles (Hunt et al., 2017). The higher internalization of LinTT1-Lipo than bare-Lipo in MDA-MB-231 cells were in agreement with previous studies that demonstrated the increased cellular uptake of LinTT1-functionalized nanoparticles in comparison with bare nanoparticles on several cancer cells, including breast cancer ones (Simón-Gracia et al., 2018b; Hunt et al., 2017).

Flow cytometry analysis (Fig. 8A) agreed with confocal analysis that qualitatively demonstrated that LinTT1-Lipo were more taken-up and internalized in 3D spheroids of MDA-MB-231 cells in a time-dependent manner (Fig. 8B). DAPI solution (blue) was used to stain the nuclei of MDA-MB-231 cells showing a spherical-like three-dimensional arrangement of spheroids (Fig. 8B). The interaction between liposomes (both bare and functionalized ones) and spheroids was evaluated using the light channel of AlexaFluor488® (green) that has the same adsorption and excitation wavelength of FAM group conjugated to peptide on LinTT1-Lipo and fluorescein group conjugated to DHPE lipid on bare-Lipo. Moreover, in agreement to flow cytometry data, the differences between bare- and LinTT1-Lipo are more significant for shorter incubation time (3 h) than longer ones (6 h), despite the interaction between LinTT1-lipo and spheroids still remained clearly higher than the interaction between bare-Lipo and spheroids after 6 h of incubation.

3.8. *Primary human M2 macrophages-liposomes interaction study*

Currently, the targeting of M2 macrophages is one of the most promising approaches to design novel anticancer nanomedicines or potentiate the existing therapies (Cassetta and Pollard, 2018). Based on the evidence that M2 macrophages have an overexpression of p32 protein (Fogal et al., 2008), we studied the interaction between LinTT1-Lipo and these specific cells. Macrophages were collected from whole human blood and then differentiated in M2 phenotype, as described in the Experimental Section. The presence of surface specific markers for M2 macrophages was evaluated using flow cytometry analysis and endorsed the proper differentiation of monocytes in M2 macrophages (Figure S12). The interaction study demonstrated that LinTT1-Lipo had a higher interaction rate with M2 macrophages than bare-Lipo at both short (1 h) and long (3 h) incubation times (Fig. 9).

After 1 h of incubation the interaction rate was 5.7 ± 2.2% and 26.5 ± 2.6% for bare-Lipo and LinTT1-Lipo, respectively, while it was 19.4 ± 3.5% and 55.4 ± 4.6% for bare-Lipo and LinTT1-Lipo, respectively, after 3 h of incubation with M2-macrophage. Differences depend on the LinTT1-peptide that is conjugated to the surface of liposomes and the links selectively p32 protein receptor overexpressed on the surface of M2 macrophages (Torrieri et al., 2020).

The effective amount of LinTT1-Lipo internalized by M2 macrophages was further studied by quenching the fluorescence of the liposomes on the cell membrane of the macrophages with trypan blue solution. No-significant differences were obtained for the specific uptake and internalization of bare-Lipo with or without quenching agent (5.7 ± 2.2% versus 4.2 ± 1.2% and 19.4 ± 3.5% versus 16.2 ± 2.8% after 1 h and 3 h of incubation, respectively) (Fig. 9). Conversely, interaction study between LinTT1-Lipo and M2-like macrophage in presence of cell membrane quenching agent demonstrated that only part of the LinTT1-Lipo were taken-up and internalized in M2 macrophages, and the other part was only strongly associated onto the cell membrane (Fig. 9). After 1 h of incubation with LinTT1-Lipo the positive events were 26.5 ± 2.6% versus 15.2 ± 2.4% and 55.4 ± 4.6% versus 27.8 ± 2.9% after 3 h of incubation, in absence and presence of the quenching agent, respectively. Based on this, M2-macrophages can improve the accumulation of LinTT1-functionalized liposomes in the hypoxic area of tumor core. Our suggestion is based on the intrinsic ability of macrophages to accumulate themselves in the hypoxic area of tumor core (where the most abundant phenotype is M2-like), as described elsewhere (Casazza et al., 2013; Silva, 2017; Zhang et al., 2014; Qiu et al., 2018; Chen et al., 2019b; Pang et al., 2016). For this reason, M2-macrophages can represent a cellular carrier for a potential delivery of LinTT1-liposomes which are strongly associated, and partially internalized by M2-macrophages, in order to increase the accumulation of liposomes in hypoxic tumor area through a

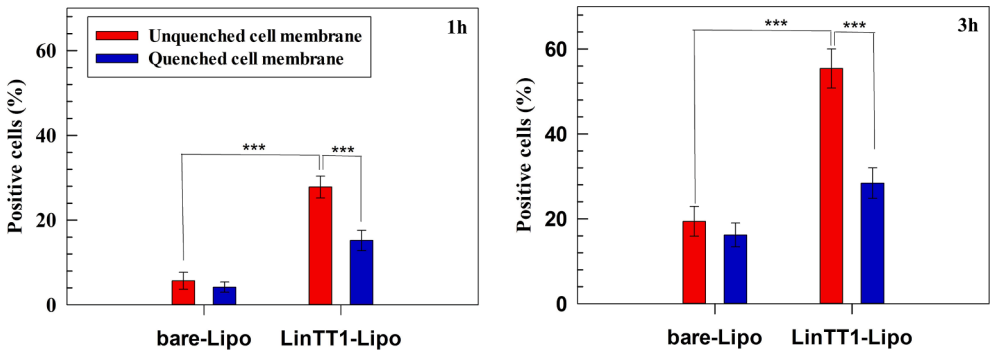

Fig. 9. Interaction between bare and/or LinTT1-functionalized liposomes and primary human M2 macrophages. Quantitative analysis was carried out by using flow cytometry analysis after 1 and 3 h of incubation. When required, a trypan blue solution was used to quench the fluorescence of the liposomes on the cell membrane. Data is the average of three independent experiments ± S.D. Statistical significance was set at: *$p < 0.05$, **$p < 0.01$, and ***$p < 0.001$.

"hitchhike-like process.

4. Conclusions

In this study, we constructed tumor-targeting nanovesicles by conjugating LinTT1 peptide to the surface of therapeutic liposomes. LinTT1-functionalized liposomes increased the therapeutic activity of two chemotherapeutic drugs, DOX and SRF, in both positive estrogen receptor (MCF-7) and triple negative breast cancer (MDA-MB-231) cells. The anticancer activity of the targeted liposomes also increased in 2D cell models compared to single chemotherapeutic drugs. LinTT1-functionalized liposomes were more internalized and taken-up in 3D spheroids of MDA-MB-231 cells than bare liposomes. The anticancer activity of DOX and SRF co-loaded LinTT1-functionalized liposomes also increased in 3D spheroids of MDA-MB-231 cells compared to both bare liposomes and combination of free drugs. LinTT1-functionalized liposomes were partly internalized and partly associated to the external cell membranes of primary M2 macrophages. The amount of LinTT1-functionalized liposomes that is associated onto the surface of primary human M2 macrophages could be used as a potential mechanism to modulate the penetration and accumulation of targeting liposomes in the central portion of the hypoxic area of tumor tissues. These promising results highlight the potential use of DOX and SRF co-loaded LinTT1-functionalized liposomes as nanomedicines for the treatment of metastatic TNB cancer.

CRediT authorship contribution statement

Nicola d'Avanzo: Conceptualization, Methodology, Investigation, Formal analysis, Visualization, Writing - original draft. **Giulia Torrieri:** Investigation. **Patrícia Figueiredo:** Investigation. **Christian Celia:** Conceptualization, Supervision, Resources, Funding acquisition, Project administration, Writing - review & editing. **Donatella Paolino:** Conceptualization, Supervision, Resources, Funding acquisition, Project administration, Writing - review & editing. **Alexandra Correia:** Investigation. **Karina Moslova:** Investigation. **Tambet Teesalu:** Conceptualization, Supervision, Resources, Funding acquisition, Project administration, Writing - review & editing. **Massimo Fresta:** Conceptualization, Supervision, Resources, Funding acquisition, Project administration, Writing - review & editing. **Hélder A. Santos:** Conceptualization, Supervision, Resources, Funding acquisition, Project administration, Writing - review & editing.

Declaration of Competing Interest

The authors declare that they have no known competing financial interests or personal relationships that could have appeared to influence the work reported in this paper.

Acknowledgements

N. d'Avanzo acknowledges support from the Italian Ministry of Education and University Magna Græcia of Catanzaro and from Fondo Giovani DM 1047/2017-D.R. n. 1017. T. Teesalu was supported by the European Union through the European Regional Development Fund (Project No. 2014-2020.4.01.15-0012), and Estonian Research Council grants PRG230 and EAG79. H. A. Santos acknowledges the financial support from Sigrid Jusélius Foundation and the HiLIFE Research Funds. The authors also acknowledge the following core facilities funded by Biocenter Finland: Confocal and flow cytometry Biocore for the use of their instruments.

Appendix A. Supplementary data

Supplementary data to this article can be found online at https://doi.org/10.1016/j.ijpharm.2021.120346.

References

Agemy, L., Kotamraju, V.R., Friedmann-Morvinski, D., Sharma, S., Sugahara, K.N., Ruoslahti, E., 2013. Proapoptotic peptide-mediated cancer therapy targeted to cell surface p32. Mol. Ther. 21, 2195–2204.
Akram, M., Iqbal, M., Daniyal, M., Khan, A.U., 2017. Awareness and current knowledge of breast cancer. Biol. Res. 50, 33.
Al-Mahmood, S., Sapiezynski, J., Garbuzenko, O.B., Minko, T., 2018. Metastatic and triple-negative breast cancer: challenges and treatment options. Drug Deliv. Transl. Res. 8, 1483–1507.
Almeida, P.V., Shahbazi, M.-A., Correia, A., Mäkilä, E., Kemell, M., Salonen, J., Hirvonen, J., Santos, H.A., 2017. A multifunctional nanocomplex for enhanced cell uptake, endosomal escape and improved cancer therapeutic effect. Nanomedicine 12, 1401–1420.
Almeida, P.V., Shahbazi, M.A., Makila, E., Kaasalainen, M., Salonen, J., Hirvonen, J., Santos, H.A., 2014. Amine-modified hyaluronic acid-functionalized porous silicon nanoparticles for targeting breast cancer tumors. Nanoscale 6, 10377–10387.
Anselmo, A.C., Mitragotri, S., 2019. Nanoparticles in the clinic: an update. Bioeng. Transl. Med. 4, e10143.
Arruebo, M., Vilaboa, N., Sáez-Gutierrez, B., Lambea, J., Tres, A., Valladares, M., González-Fernández, Á., 2011. Assessment of the evolution of cancer treatment therapies. Cancers 3, 3279–3330.
Barenholz, Y., 2012. Doxil(R)–the first FDA-approved nano-drug: lessons learned. J. Contr. Release 160, 117–134.
Barone, A., Cristiano, M.C., Cilurzo, F., Locatelli, M., Iannotta, D., Di Marzio, L., Celia, C., Paolino, D., 2020. Ammonium glycyrrhizate skin delivery from ultradeformable liposomes: a novel use as an anti-inflammatory agent in topical drug delivery. Colloids Surf. B: Biointerf. 193, 111152.
Barone, A., Mendes, M., Cabral, C., Mare, R., Paolino, D., Vitorino, C., 2019. Hybrid nanostructured films for topical administration of simvastatin as coadjuvant treatment of melanoma. J. Pharm. Sci. 108, 3396–3407.
Behzadi, S., Vatan, N.M., Lema, K., Nwaobasi, D., Zenkov, I., Abadi, P.P., Khan, D.A., Corbo, C., Aghaverdi, H., Farokhzad, O.C., 2018. Flat cell culturing surface may cause misinterpretation of cellular uptake of nanoparticles. Adv. Biosyst. 2, 1800046.
Bhatt, P., Lalani, R., Vhora, I., Patil, S., Amrutiya, J., Misra, A., Mashru, R., 2018. Liposomes encapsulating native and cyclodextrin enclosed paclitaxel: enhanced loading efficiency and its pharmacokinetic evaluation. Int. J. Pharm. 536, 95–107.

Blanco, E., Shen, H., Ferrari, M., 2015. Principles of nanoparticle design for overcoming biological barriers to drug delivery. Nat. Biotechnol. 33, 941.
Bloor, J., Morrison, J., Rhodes, C., 1970. Effect of pH on the micellar properties of a nonionic surfactant. J. Pharm. Sci. 59, 387–391.
Bozzuto, G., Molinari, A., 2015. Liposomes as nanomedical devices. Int. J. Nanomed. 10, 975.
Braun, G.B., Sugahara, K.N., Olivia, M.Y., Kotamraju, V.R., Mölder, T., Lowy, A.M., Ruoslahti, E., Teesalu, T., 2016. Urokinase-controlled tumor penetrating peptide. J. Contr. Release 232, 188–195.
Bray, F., Ferlay, J., Soerjomataram, I., Siegel, R.L., Torre, L.A., Jemal, A., 2018. Global cancer statistics 2018: GLOBOCAN estimates of incidence and mortality worldwide for 36 cancers in 185 countries. CA: A Cancer J. Clin. 68, 394–424.
Bronte, G., Andreis, D., Bravaccini, S., Maltoni, R., Cecconetto, L., Schirone, A., Farolfi, A., Fedeli, A., Serra, P., Donati, C., 2017. Sorafenib for the treatment of breast cancer. Exp. Opin. Pharmacother. 18, 621–630.
Bulbake, U., Doppalapudi, S., Kommineni, N., Khan, W., 2017. Liposomal formulations in clinical use: an updated review. Pharmaceutics 9, 12.
Caddeo, C., Pucci, L., Gabriele, M., Carbone, C., Fernàndez-Busquets, X., Valenti, D., Pons, R., Vassallo, A., Fadda, A.M., Manconi, M., 2018. Stability, biocompatibility and antioxidant activity of PEG-modified liposomes containing resveratrol. Int. J. Pharm. 538, 40–47.
Cai, D., Gao, W., He, B., Dai, W., Zhang, H., Wang, X., Wang, J., Zhang, X., Zhang, Q., 2014. Hydrophobic penetrating peptide PFVYLI-modified stealth liposomes for doxorubicin delivery in breast cancer therapy. Biomaterials 35, 2283–2294.
Casazza, A., Laoui, D., Wenes, M., Rizzolio, S., Bassani, N., Mambretti, M., Deschoemaeker, S., Van Ginderachter, J.A., Tamagnone, L., Mazzone, M., 2013. Impeding macrophage entry into hypoxic tumor areas by Sema3A/Nrp1 signaling blockade inhibits angiogenesis and restores antitumor immunity. Cancer Cell 24, 695–709.
Cassetta, L., Pollard, J.W., 2018. Targeting macrophages: therapeutic approaches in cancer. Nat. Rev. Drug Discov. 17, 887–904.
Celia, C., Cristiano, M.C., Froiio, F., Di Francesco, M., d'Avanzo, N., Di Marzio, L., Fresta, M., 2021. Nanoliposomes as multidrug carrier of gemcitabine/paclitaxel for the effective treatment of metastatic breast cancer disease: a comparison with Gemzar and Taxol. Adv. Therapeut. 4, 2000121.
Celia, C., Trapasso, E., Cosco, D., Paolino, D., Fresta, M., 2009. Turbiscan Lab® Expert analysis of the stability of ethosomes® and ultradeformable liposomes containing a bilayer fluidizing agent. Colloids Surf. B: Biointerf. 72, 155–160.
Cern, A., Barenholz, Y., Tropsha, A., Goldblum, A., 2014. Computer-aided design of liposomal drugs: in silico prediction and experimental validation of drug candidates for liposomal remote loading. J. Contr. Release 173, 125–131.
Cern, A., Marcus, D., Tropsha, A., Barenholz, Y., Goldblum, A., 2017. New drug candidates for liposomal delivery identified by computer modeling of liposomes' remote loading and leakage. J. Contr. Release 252, 18–27.
Charrois, G.J., Allen, T.M., 2004. Drug release rate influences the pharmacokinetics, biodistribution, therapeutic activity, and toxicity of pegylated liposomal doxorubicin formulations in murine breast cancer. Biochim. Biophys. Acta (BBA)-Biomembr. 1663, 167-177.
Chavez-MacGregor, M., Mittendorf, E.A., Clarke, C.A., Lichtensztajn, D.Y., Hunt, K.K., Giordano, S.H., 2017. Incorporating tumor characteristics to the American Joint Committee on Cancer breast cancer staging system. Oncologist 22, 1292.
Chen, H., Lu, W., Zhang, Y., Zhu, X., Zhou, J., Chen, Y., 2019a. A Bayesian network meta-analysis of the efficacy of targeted therapies and chemotherapy for treatment of triple-negative breast cancer. Cancer Med. 8, 383–399.
Chen, Y., Song, Y., Du, W., Gong, L., Chang, H., Zou, Z., 2019b. Tumor-associated macrophages: an accomplice in solid tumor progression. J. Biomed. Sci. 26, 1–13.
Chen, Y.B., Jiang, C.T., Zhang, G.Q., Wang, J.S., Pang, D., 2009. Increased expression of hyaluronic acid binding protein 1 is correlated with poor prognosis in patients with breast cancer. J. Surg. Oncol. 100, 382–386.
Cheung, C.C., Al-Jamal, W.T., 2019. Sterically stabilized liposomes production using staggered herringbone micromixer: effect of lipid composition and PEG-lipid content. Int. J. Pharm. 566, 687–696.
Cosco, D., Paolino, D., Cilurzo, F., Casale, F., Fresta, M., 2012. Gemcitabine and tamoxifen-loaded liposomes as multidrug carriers for the treatment of breast cancer diseases. Int. J. Pharm. 422, 229–237.
Cosco, D., Paolino, D., Maiuolo, J., Russo, D., Fresta, M., 2011. Liposomes as multicompartmental carriers for multidrug delivery in anticancer chemotherapy. Drug Deliv. Transl. Res. 1, 66–75.
Costanzo, M., Vurro, F., Cisterna, B., Boschi, F., Marengo, A., Montanari, E., Meo, C.D., Matricardi, P., Berlier, G., Stella, B., 2019. Uptake and intracellular fate of biocompatible nanocarriers in cycling and noncycling cells. Nanomedicine 14, 301–316.
Dafni, U., Tsourti, Z., Alatsathianos, I., 2019. Breast cancer statistics in the European Union: incidence and survival across European countries. Breast Care 14, 344–353.
d'Avanzo, N., Celia, C., Barone, A., Carafa, M., Di Marzio, L., Santos, H.A., Fresta, M., 2020. Immunogenicity of polyethylene glycol based nanomedicines: mechanisms, clinical implications and systematic approach. Adv. Therapeut. 3, 1900170.
de la Harpe, K.M., Kondiah, P.P., Choonara, Y.E., Marimuthu, T., du Toit, L.C., Pillay, V., 2019. The hemocompatibility of nanoparticles: a review of cell-nanoparticle interactions and hemostasis. Cells 8, 1209.
DeSantis, C.E., Ma, J., Gaudet, M.M., Newman, L.A., Miller, K.D., Goding Sauer, A., Jemal, A., Siegel, R.L., 2019. Breast cancer statistics, 2019. CA: A Cancer J. Clin. 69, 438-451.
Di Francesco, M., Celia, C., Cristiano, M.C., d'Avanzo, N., Ruozi, B., Mircioiu, C., Cosco, D., Di Marzio, L., Fresta, M., 2021. Doxorubicin hydrochloride-loaded nonionic surfactant vesicles to treat metastatic and non-metastatic breast cancer. ACS Omega 6, 2973–2989.
Di Francesco, M., Celia, C., Primavera, R., D'Avanzo, N., Locatelli, M., Fresta, M., Cilurzo, F., Ventura, C.A., Paolino, D., Di Marzio, L., 2017a. Physicochemical characterization of pH-responsive and fusogenic self-assembled non-phospholipid vesicles for a potential multiple targeting therapy. Int. J. Pharm. 528, 18–32.
Di Francesco, M., Primavera, R., Fiorito, S., Cristiano, M.C., Taddeo, V.A., Epifano, F., Di Marzio, L., Genovese, S., Celia, C., 2017b. Acronychiabaueri analogue derivative-loaded ultradeformable vesicles: physicochemical characterization and potential applications. Planta Med. 83, 482–491.
Di Wu, M.S., Xue, H.-Y., Wong, H.-L., 2017. Nanomedicine applications in the treatment of breast cancer: current state of the art. Int. J. Nanomed. 12, 5879.
Du, M., Ouyang, Y., Meng, F., Ma, Q., Liu, H., Zhuang, Y., Pang, M., Cai, T., Cai, Y., 2019. Nanotargeted agents: an emerging therapeutic strategy for breast cancer. Nanomedicine 14, 1771–1786.
Ferrari, M., 2010. Frontiers in cancer nanomedicine: directing mass transport through biological barriers. Trends Biotechnol. 28, 181–188.
Figueiredo, P., Sipponen, M.H., Lintinen, K., Correia, A., Kiriazis, A., Yli-Kauhaluoma, J., Österberg, M., George, A., Hirvonen, J., Kostiainen, M.A., 2019. Preparation and characterization of dentin phosphophoryn-derived peptide-functionalized lignin nanoparticles for enhanced cellular uptake. Small 15, 1901427.
Fisusi, F.A., Akala, E.O., 2019. Drug combinations in breast cancer therapy. Pharm. Nanotechnol. 7, 3–23.
Fogal, V., Zhang, L., Krajewski, S., Ruoslahti, E., 2008. Mitochondrial/cell-surface protein p32/gC1qR as a molecular target in tumor cells and tumor stroma. Cancer Res. 68, 7210–7218.
Fritze, A., Hens, F., Kimpfler, A., Schubert, R., Peschka-Süss, R., 2006. Remote loading of doxorubicin into liposomes driven by a transmembrane phosphate gradient. Biochim. Biophys. Acta (BBA)-Biomembr. 1758, 1633-1640.
Frohlich, E., 2018. Comparison of conventional and advanced in vitro models in the toxicity testing of nanoparticles. Artif. Cells Nanomed. Biotechnol. 46, 1091–1107.
Guo, Y., Zhong, T., Duan, X.-C., Zhang, S., Yao, X., Yin, Y.-F., Huang, D., Ren, W., Zhang, Q., Zhang, X., 2017. Improving anti-tumor activity of sorafenib tosylate by lipid-and polymer-coated nanomatrix. Drug Deliv. 24, 270–277.
Hadjidemetriou, M., McAdam, S., Garner, G., Thackeray, C., Knight, D., Smith, D., Al-Ahmady, Z., Mazza, M., Rogan, J., Clamp, A., 2019. The human in vivo biomolecule corona onto PEGylated liposomes: a proof-of-concept clinical study. Adv. Mater. 31, 1803335.
Hawkes, N., 2019. Cancer survival data emphasise importance of early diagnosis. Br. Med. J. Publ. Group.
Hunt, H., Simón-Gracia, L., Tobi, A., Kotamraju, V.R., Sharma, S., Nigul, M., Sugahara, K. N., Ruoslahti, E., Teesalu, T., 2017. Targeting of p32 in peritoneal carcinomatosis with intraperitoneal linTT1 peptide-guided pro-apoptotic nanoparticles. J. Contr. Release 260, 142–153.
Hwang, S.-Y., Park, S., Kwon, Y., 2019. Recent therapeutic trends and promising targets in triple negative breast cancer. Pharmacol. Therapeut. 199, 30–57.
Immordino, M.L., Dosio, F., Cattel, L., 2006. Stealth liposomes: review of the basic science, rationale, and clinical applications, existing and potential. Int. J. Nanomed. 1, 297.
Justus, C.R., Dong, L., Yang, L.V., 2013. Acidic tumor microenvironment and pH-sensing G protein-coupled receptors. Front. Physiol. 4, 354.
Kalluri, R., Zeisberg, M., 2006. Fibroblasts in cancer. Nat. Rev. Cancer 6, 392–401.
Keating, G.M., 2017. Sorafenib: a review in hepatocellular carcinoma. Targeted Oncol. 12, 243–253.
Khan, D.R., Webb, M.N., Cadotte, T.H., Gavette, M.N., 2015. Use of targeted liposome-based chemotherapeutics to treat breast cancer. Breast Cancer: Basic Clin. Res. 9, BCBCR. S29421.
Khosravi-Shahi, P., Cabezón-Gutiérrez, L., Aparicio Salcedo, M.I., 2019. State of art of advanced triple negative breast cancer. Breast J. 25, 967–970.
Laakkonen, P., Vuorinen, K., 2010. Homing peptides as targeted delivery vehicles. Integr. Biol. 2, 326–337.
Lee, A., Djamgoz, M.B.A., 2018. Triple negative breast cancer: emerging therapeutic modalities and novel combination therapies. Cancer Treat. Rev. 62, 110–122.
Lei, M., Ma, G., Sha, S., Wang, X., Feng, H., Zhu, Y., Du, X., 2019. Dual-functionalized liposome by co-delivery of paclitaxel with sorafenib for synergistic antitumor efficacy and reversion of multidrug resistance. Drug Deliv. 26, 262–272.
Li, C., Lai, C., Qiu, Q., Luo, X., Hu, L., Zheng, H., Lu, Y., Liu, M., Zhang, H., Liu, X., 2019. Dual-ligand modification of PEGylated liposomes used for targeted doxorubicin delivery to enhance anticancer efficacy. AAPS PharmSciTech 20, 1–13.
Lovitt, C.J., Shelper, T.B., Avery, V.M., 2018. Doxorubicin resistance in breast cancer cells is mediated by extracellular matrix proteins. BMC Cancer 18, 41.
Luo, S., Feng, J., Xiao, L., Guo, L., Deng, L., Du, Z., Xue, Y., Song, X., Sun, X., Zhang, Z., 2020. Targeting self-assembly peptide for inhibiting breast tumor progression and metastasis. Biomaterials 120055.
Maggisano, V., Celano, M., Malivindi, R., Barone, I., Cosco, D., Mio, C., Mignogna, C., Panza, S., Damante, G., Fresta, M., Ando, S., Russo, D., Catalano, S., Bulotta, S., 2019. Nanoparticles loaded with the BET inhibitor JQ1 block the growth of triple negative breast cancer cells In vitro and in vivo. Cancers (Basel) 12, 91.
Maruyama, K., 2011. Intracellular targeting delivery of liposomal drugs to solid tumors based on EPR effects. Adv. Drug Deliv. Rev. 63, 161–169.
Masoud, V., Pagès, G., 2017. Targeted therapies in breast cancer: new challenges to fight against resistance. World J. Clin. Oncol. 8, 120.
Meng, J., Guo, F., Xu, H., Liang, W., Wang, C., Yang, X.-D., 2016. Combination therapy using co-encapsulated resveratrol and paclitaxel in liposomes for drug resistance reversal in breast cancer cells in vivo. Sci. Rep. 6, 22390.

Mima, Y., Lila, A.S.A., Shimizu, T., Ukawa, M., Ando, H., Kurata, Y., Ishida, T., 2017. Ganglioside inserted into PEGylated liposome attenuates anti-PEG immunity. J. Contr. Release 250, 20–26.
Monopoli, M.P., Åberg, C., Salvati, A., Dawson, K.A., 2012. Biomolecular coronas provide the biological identity of nanosized materials. Nat. Nanotechnol. 7, 779–786.
Olusanya, T.O., Ahmad, H., Rushdi, R., Ibegbu, D.M., Smith, J.R., Elkordy, A.A., 2018. Liposomal drug delivery systems and anticancer drugs. Molecules 23, 907.
Paasonen, L., Sharma, S., Braun, G.B., Kotamraju, V.R., Chung, T.D., She, Z.G., Sugahara, K.N., Yliperttula, M., Wu, B., Pellecchia, M., Ruoslahti, E., Teesalu, T., 2016. New p32/gC1qR ligands for targeted tumor drug delivery. ChemBioChem 17, 570–575.
Palange, A.L., Di Mascolo, D., Carallo, C., Gnasso, A., Decuzzi, P., 2014. Lipid–polymer nanoparticles encapsulating curcumin for modulating the vascular deposition of breast cancer cells. Nanomed.: Nanotechnol. Biol. Med. 10, e991–e1002.
Palchetti, S., Colapicchioni, V., Digiacomo, L., Caracciolo, G., Pozzi, D., Capriotti, A.L., La Barbera, G., Laganà, A., 2016. The protein corona of circulating PEGylated liposomes. Biochim. Biophys. Acta (BBA)-Biomembr. 1858, 189–196.
Pang, L., Qin, J., Han, L., Zhao, W., Liang, J., Xie, Z., Yang, P., Wang, J., 2016. Exploiting macrophages as targeted carrier to guide nanoparticles into glioma. Oncotarget 7, 37081.
Paolino, D., Accolla, M.L., Cilurzo, F., Cristiano, M.C., Cosco, D., Castelli, F., Sarpietro, M.G., Fresta, M., Celia, C., 2017. Interaction between PEG lipid and DSPE/DSPC phospholipids: an insight of PEGylation degree and kinetics of de-PEGylation. Colloids Surf. B: Biointerf. 155, 266–275.
Paolino, D., Cosco, D., Gaspari, M., Celano, M., Wolfram, J., Voce, P., Puxeddu, E., Filetti, S., Celia, C., Ferrari, M., 2014. Targeting the thyroid gland with thyroid-stimulating hormone (TSH)-nanoliposomes. Biomaterials 35, 7101–7109.
Park, J.E., Dutta, B., Tse, S.W., Gupta, N., Tan, C.F., Low, J.K., Yeoh, K.W., Kon, O.L., Tam, J.P., Sze, S.K., 2019. Hypoxia-induced tumor exosomes promote M2-like macrophage polarization of infiltrating myeloid cells and microRNA-mediated metabolic shift. Oncogene 38, 5158–5173.
Pasut, G., Paolino, D., Celia, C., Mero, A., Joseph, A.S., Wolfram, J., Cosco, D., Schiavon, O., Shen, H., Fresta, M., 2015. Polyethylene glycol (PEG)-dendron phospholipids as innovative constructs for the preparation of super stealth liposomes for anticancer therapy. J. Contr. Release 199, 106–113.
Peerschke, E.I., Ghebrehiwet, B., 2014. cC1qR/CR and gC1qR/p33: observations in cancer. Mol. Immunol. 61, 100–109.
Peerschke, E.I., Li, X., Eguchi, T., Aly, R., Chintala, N.K., Tan, K.S., Zauderer, M.G., Dembitzer, F.R., Beasley, M.B., Ghebrehiwet, B., 2019. Globular C1q receptor (gC1qR/p32/HABP1) is overexpressed in malignant pleural mesothelioma and is associated with increased survival in patients treated with chemotherapy. Front. Oncol. 9, 1042.
Pitoia, F., Jerkovich, F., 2016. Selective use of sorafenib in the treatment of thyroid cancer. Drug Des. Devel. Ther. 10, 1119.
Pozzi, D., Caracciolo, G., Digiacomo, L., Colapicchioni, V., Palchetti, S., Capriotti, A., Cavaliere, C., Chiozzi, R.Z., Puglisi, A., Laganà, A., 2015. The biomolecular corona of nanoparticles in circulating biological media. Nanoscale 7, 13958–13966.
Pretini, V., Koenen, M.H., Kaestner, L., Fens, M.H., Schiffelers, R.M., Bartels, M., Van Wijk, R., 2019. Red blood cells: chasing interactions. Front. Physiol. 10, 945.
Pu, Y., Zhang, H., Peng, Y., Fu, Q., Yue, Q., Zhao, Y., Guo, L., Wu, Y., 2019. Dual-targeting liposomes with active recognition of GLUT5 and αvβ3 for triple-negative breast cancer. Eur. J. Med. Chem. 183, 111720.
Qiu, S.-Q., Waaijer, S.J., Zwager, M.C., de Vries, E.G., van der Vegt, B., Schröder, C.P., 2018. Tumor-associated macrophages in breast cancer: innocent bystander or important player? Cancer Treat. Rev. 70, 178–189.
Qu, X., Qiu, P., Zhu, Y., Yang, M., Mao, C., 2017. Guiding nanomaterials to tumors for breast cancer precision medicine: from tumor-targeting small-molecule discovery to targeted nanodrug delivery. NPG Asia Mater. 9 e452 e452.
Riaz, M.K., Riaz, M.A., Zhang, X., Lin, C., Wong, K.H., Chen, X., Zhang, G., Lu, A., Yang, Z., 2018. Surface functionalization and targeting strategies of liposomes in solid tumor therapy: a review. Int. J. Mol. Sci. 19, 195.
Rubinstein, D.B., Stortchevoi, A., Boosalis, M., Ashfaq, R., Ghebrehiwet, B., Peerschke, E. I., Calvo, F., Guillaume, T., 2004. Receptor for the globular heads of C1q (gC1q-R, p33, hyaluronan-binding protein) is preferentially expressed by adenocarcinoma cells. Int. J. Cancer 110, 741–750.
Rustamov, V., Keller, F., Klicks, J., Hafner, M., Rudolf, R., 2019. Bone sialoprotein shows enhanced expression in early, high-proliferation stages of three-dimensional spheroid cell cultures of breast cancer cell line MDA-MB-231. Front. Oncol. 9, 36.
Saha, P., Datta, K., 2018. Multi-functional, multicompartmental hyaluronan-binding protein 1 (HABP1/p32/gC1qR): implication in cancer progression and metastasis. Oncotarget 9, 10784–10807.
Sahai, E., Astsaturov, I., Cukierman, E., DeNardo, D.G., Egeblad, M., Evans, R.M., Fearon, D., Greten, F.R., Hingorani, S.R., Hunter, T., Hynes, R.O., Jain, R.K., Janowitz, T., Jorgensen, C., Kimmelman, A.C., Kolonin, M.G., Maki, R.G., Powers, R. S., Pure, E., Ramirez, D.C., Scherz-Shouval, R., Sherman, M.H., Stewart, S., Tlsty, T. D., Tuveson, D.A., Watt, F.M., Weaver, V., Weeraratna, A.T., Werb, Z., 2020. A framework for advancing our understanding of cancer-associated fibroblasts. Nat. Rev. Cancer 20, 174–186.
Sercombe, L., Veerati, T., Moheimani, F., Wu, S.Y., Sood, A.K., Hua, S., 2015. Advances and challenges of liposome assisted drug delivery. Front. Pharmacol. 6, 286.
Shahbazi, M.-A., Hamidi, M., Mäkilä, E.M., Zhang, H., Almeida, P.V., Kaasalainen, M., Salonen, J.J., Hirvonen, J.T., Santos, H.A., 2013. The mechanisms of surface chemistry effects of mesoporous silicon nanoparticles on immunotoxicity and biocompatibility. Biomaterials 34, 7776–7789.
Sharma, S., Kotamraju, V.R., Molder, T., Tobi, A., Teesalu, T., Ruoslahti, E., 2017. Tumor-penetrating nanosystem strongly suppresses breast tumor growth. Nano Lett. 17, 1356–1364.
Shibata, H., Izutsu, K.-I., Yomota, C., Okuda, H., Goda, Y., 2015. Investigation of factors affecting in vitro doxorubicin release from PEGylated liposomal doxorubicin for the development of in vitro release testing conditions. Drug Devel. Ind. Pharm. 41, 1376–1386.
Siegel, R.L., Miller, K.D., Jemal, A., 2020. Cancer statistics, 2020. CA: A Cancer J. Clin. 70, 7-30.
Silva, V.L., 2017. Exploiting the cancer niche: tumor-associated macrophages and hypoxia as promising synergistic targets for nano-based therapy. J. Contr. Release 253, 82–96.
Simón-Gracia, L., Hunt, H., Teesalu, T., 2018a. Peritoneal carcinomatosis targeting with tumor homing peptides. Molecules 23, 1190.
Simón-Gracia, L., Scodeller, P., Fuentes, S.S., Vallejo, V.G., Ríos, X., San Sebastián, E., Sidorenko, V., Di Silvio, D., Suck, M., De Lorenzi, F., 2018b. Application of polymersomes engineered to target p32 protein for detection of small breast tumors in mice. Oncotarget 9, 18682.
Singh, M.K., Pindiprolu, S.K.S., Sanapalli, B.K.R., Yele, V., Ganesh, G., 2019. Tumor homing peptide modified liposomes of capecitabine for improved apoptotic activity and HER2 targeted therapy in breast cancer: in vitro studies. RSC Adv. 9, 24987–24994.
Song, N., Zhao, L., Zhu, M., Zhao, J., 2019. Recent progress in LyP-1-based strategies for targeted imaging and therapy. Drug Deliv. 26, 363–375.
Sui, J., Cui, Y., Cai, H., Bian, S., Xu, Z., Zhou, L., Sun, Y., Liang, J., Fan, Y., Zhang, X., 2017. Synergistic chemotherapeutic effect of sorafenib-loaded pullulan-Dox conjugate nanoparticles against murine breast carcinoma. Nanoscale 9, 2755–2767.
Tahir, N., Madni, A., Li, W., Correia, A., Khan, M.M., Rahim, M.A., Santos, H.A., 2020. Microfluidic fabrication and characterization of sorafenib-loaded lipid-polymer hybrid nanoparticles for controlled drug delivery. Int. J. Pharm. 581, 119275.
Tai, K., Liu, F., He, X., Ma, P., Mao, L., Gao, Y., Yuan, F., 2018. The effect of sterol derivatives on properties of soybean and egg yolk lecithin liposomes: stability, structure and membrane characteristics. Food Res. Int. 109, 24–34.
Tampaki, E.C., Tampakis, A., Alifieris, C.E., Krikelis, D., Pazaiti, A., Kontos, M., Trafalis, D.T., 2018. Efficacy and safety of neoadjuvant treatment with bevacizumab, liposomal doxorubicin, cyclophosphamide and paclitaxel combination in locally/regionally advanced, HER2-negative, grade III at premenopausal status breast cancer: a phase II study. Clin. Drug Invest. 38, 639–648.
Torrieri, G., Fontana, F., Figueiredo, P., Liu, Z., Ferreira, M., Talman, V., Martins, J.P., Fusciello, M., Moslova, K., Ceullo, V., 2020. Dual-peptide functionalized acetalated dextran-based nanoparticles for sequential targeting of macrophages during myocardial infarction. Nanoscale 12, 2350–2358.
Tremont, A., Lu, J., Cole, J.T., 2017. Endocrine therapy for early breast cancer: updated review. Ochsner J. 17, 405–411.
Unnam, S., Panduragaiah, V.M., Sidramappa, M.A., Eswara, M., Rao, B., 2019. Gemcitabine-loaded folic acid tagged liposomes: improved pharmacokinetic and bBiodistribution profile. Curr. Drug Deliv. 16, 111–122.
Vakili-Ghartavol, R., Rezayat, S.M., Faridi-Majidi, R., Sadri, K., Jaafari, M.R., 2020. Optimization of docetaxel loading conditions in liposomes: proposing potential products for metastatic breast carcinoma chemotherapy. Sci. Rep. 10, 1–14.
Vergallo, C., Torrieri, G., Provenzani, R., Miettinen, S., Moslova, K., Varjosalo, M., Cristiano, M.C., Fresta, M., Celia, C., Santos, H.A., 2020. Design, synthesis and characterization of a PEGylated stanozolol for potential therapeutic applications. Int. J. Pharm. 573, 118826.
Vlieghe, P., Lisowski, V., Martinez, J., Khrestchatisky, M., 2010. Synthetic therapeutic peptides: science and market. Drug Discov. Today 15, 40–56.
Wahba, H.A., El-Hadaad, H.A., 2015. Current approaches in treatment of triple-negative breast cancer. Cancer Biol. Med. 12, 106.
Waks, A.G., Winer, E.P., 2019. Breast cancer treatment: a review. JAMA 321, 288–300.
Wang, L., 2017. Early diagnosis of breast cancer. Sensors 17, 1572.
Wang, X., Meng, N., Wang, S., Zhang, Y., Lu, L., Wang, R., Ruan, H., Jiang, K., Wang, H., Ran, D., 2019. Non-immunogenic, low-toxicity and effective glioma targeting MTI-31 liposomes. J. Contr. Release 316, 381–392.
Wei, M., Guo, X., Tu, L., Zou, Q., Li, Q., Tang, C., Chen, B., Xu, Y., Wu, C., 2015. Lactoferrin-modified PEGylated liposomes loaded with doxorubicin for targeting delivery to hepatocellular carcinoma. Int. J. Nanomed. 10, 5123.
Wicki, A., Witzigmann, D., Balasubramanian, V., Huwyler, J., 2015. Nanomedicine in cancer therapy: challenges, opportunities, and clinical applications. J. Contr. Release 200, 138–157.
Wilhelm, S., Carter, C., Lynch, M., Lowinger, T., Dumas, J., Smith, R.A., Schwartz, B., Simantov, R., Kelley, S., 2006. Discovery and development of sorafenib: a multikinase inhibitor for treating cancer. Nat. Rev. Drug Discov. 5, 835–844.
Wolfram, J., Suri, K., Huang, Y., Molinaro, R., Borsoi, C., Scott, B., Boom, K., Paolino, D., Fresta, M., Wang, J., 2014a. Evaluation of anticancer activity of celastrol liposomes in prostate cancer cells. J. Microencapsul. 31, 501–507.
Wolfram, J., Suri, K., Yang, Y., Shen, J., Celia, C., Fresta, M., Zhao, Y., Shen, H., Ferrari, M., 2014b. Shrinkage of pegylated and non-pegylated liposomes in serum. Colloids Surf. B: Biointerf. 114, 294–300.
Xiao, Y., Liu, Y., Yang, S., Zhang, B., Wang, T., Jiang, D., Zhang, J., Yu, D., Zhang, N., 2016. Sorafenib and gadolinium co-loaded liposomes for drug delivery and MRI-guided HCC treatment. Colloids Surf. B: Biointerf. 141, 83–92.
Yan, W., Leung, S.S., To, K.K., 2020. Updates on the use of liposomes for active tumor targeting in cancer therapy. Nanomedicine 15, 303–318.
Yardley, D.A., 2013. Drug resistance and the role of combination chemotherapy in improving patient outcomes. Int. J. Breast Cancer 2013.

Yong, T., Zhang, X., Bie, N., Zhang, H., Zhang, X., Li, F., Hakeem, A., Hu, J., Gan, L., Santos, H.A., Yang, X., 2019. Tumor exosome-based nanoparticles are efficient drug carriers for chemotherapy. Nat. Commun. 10, 3838.
Yu, T., Malugin, A., Ghandehari, H., 2011. Impact of silica nanoparticle design on cellular toxicity and hemolytic activity. ACS Nano 5, 5717–5728.
Zhang, J., Cao, J., Ma, S., Dong, R., Meng, W., Ying, M., Weng, Q., Chen, Z., Ma, J., Fang, Q., 2014. Tumor hypoxia enhances non-small cell lung cancer metastasis by selectively promoting macrophage M2 polarization through the activation of ERK signaling. Oncotarget 5, 9664.
Zhang, J., Wang, Y., Zhang, S., You, G.-X., Li, P.-L., Wang, Q., Yu, W.-L., Hu, T., Zhou, H., Zhao, L., 2018. In vitro and in vivo investigation of the novel Dex-bHb as oxygen carriers. Artif. Cells Nanomed. Biotechnol. 46, S133–S137.
Zhao, Z., Ukidve, A., Krishnan, V., Mitragotri, S., 2019. Effect of physicochemical and surface properties on in vivo fate of drug nanocarriers. Adv. Drug Deliv. Rev. 143, 3–21.